Asklepios: A Multi-Ducted Fan Based Convertible Body-Tilt Aircraft

VFS 2025 UAV for Medical Equipment Distribution

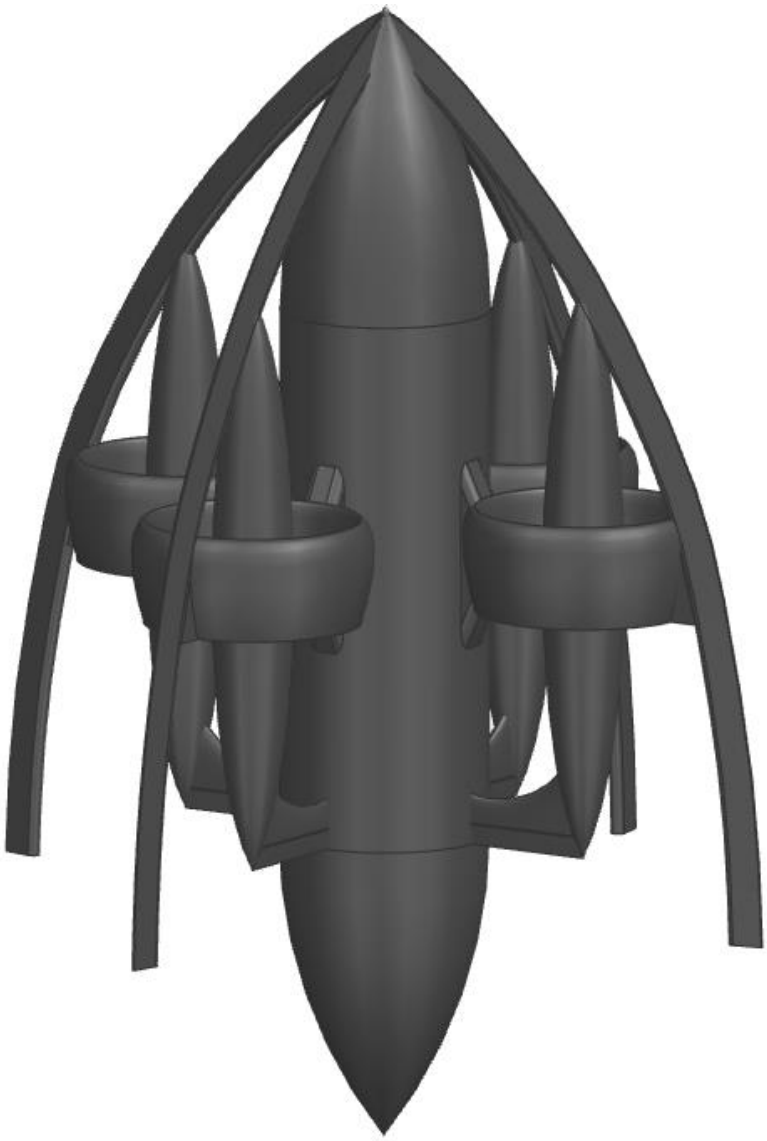

THE UNIVERSITY OF KANSAS

Department of Aerospace Engineering

May 2021

Acknowledgments:

The authors of this report would also like to acknowledge and thank our Faculty Advisor, Dr. Barrett, for his continued guidance, assistance, and comradarie throughout the report writing process.

Signature Page:

Zack Schwab

Author Email: zack.schwab@ku.edu Member ID: 24656

Mason Denneler

Author Email: masondenneler@ku.edu Member ID: 24657

Micaela Crispin

Author Email: micaela_crispin@icloud.com

Ron Barrett

Faculty Advisor Email: adaptivebarrett@gmail.com

Posting Permission Page:

I, Zachary Schwab, give the Vertical Flight Society permission to post this report online.

I, Mason Demeler, give the Vertical Flight Society permission to post this report online.

I, Micaela Crispin give the Vertical Flight Society permission to post this report online.

Table of Contents

List of Figures

List of Tables

Nomenclature

Symbol	Description	Units
A	Cumulative Duct Area	m^2
AO_k	Ancillary Objective Weighting Function	~
AR	Aspect Ratio	~
b_{duct}	Duct Span	mm
$\bar{c}$	Mean Geometric Cord	m
C_D	Finite Drag Coefficient	~
c_{duct}	Cord	mm
c_j	Specific Fuel Consumption	kg/hr-N
C_L	Finite Lift Coefficient	~
D_r	Rotor Blade Diameter	mm
E	Endurance	min
e	Oswald Efficiency Number	~
f	Parasite Area	m^2 FM
FM	Figure of Merit	~
L/D	Lift to Drag Ratio	~
M_{ff}	Mission Fuel Fraction	~
O_i	Objective Weighting Function	~
P	Power	kg-m/min
$\bar{q}$	Dynamic Pressure	Pa
R_{cr}	Cruise Range	km
R_i	Requirement Weighting Function	~
S	Reference Area	m^2
S_{wet}	Wetted Area	m^2
T	Cumulative Rotor Thrust in Hover	N
V	Cruise Speed	km/hr
$\bar{V}$	Volume Coefficient	~
W/P	Power loading	min/m
W/S	Wing loading	kg/m^2
W_e	Empty Weight	kg
W_f	Fuel Weight	kg
W_{pl}	Payload Weight	kg

W_{TO} ..... Takeoff Weight ..... kg

x_F ..... Grid Fin Displacement from CG ..... m

Greek Symbol	Description	Units

η_p ..... Rotor Efficiency ..... ~

ρ ..... Air Density ..... kg/m^3

Abbreviations

AAA ..... Advanced Aircraft Analysis .....

$BEMT$ ..... Blade Element Momentum Theory .....

CAD .....Computer Aided Design.....

CG ..... Center of Gravity .....

FAA ..... Federal Aviation Administration .....

$HIGE$ ..... Hover in Ground Effect .....

$HOGE$ ..... Hover out of Ground Effect .....

MCP ..... Maximum Continuous Power .....

MRP ..... Maximum Rated Power .....

OEI ..... One Engine Inoperative .....

RFP ..... Request for Proposal .....

SAE ..... Society of Automotive Engineers .....

$STAMPED$..... Statistical Time and Market Predictive Engineering Design .....

UAV ..... Unmanned Aerial Vehicle .....

VFR ..... Visual Flight Rules .....

VFS ..... Vertical Flight Society .....

$VTOL$ ..... Vertical Takeoff and Landing .....

1. INTRODUCTION, MISSION SPECIFICATION AND PROFILE

The goal of the VFS competition is to design an unmanned VTOL aerial vehicle capable of making fast deliveries while carrying payloads of 50 kg to customer sites at a 50 km radius, and to logistic sites up to 200 km away. The rise of the global pandemic, Covid-19, has created a demand for said fast delivery unmanned VTOL aerial vehicles. Moreover, it is stated in the RFP that, "The sizing is such that the vehicle can make a difference within a future pandemic or natural disaster."

The mission specification for both delivery types, local delivery and logistics, has been taken and modified from the RFP (Ref. 2) and are shown in Table 1.1 and Table 1.2. From the RFP/mission specification, the design chosen for the VFS competition will be a convertible body-tilt aircraft. Additionally, the mission specification will be used to size the convertible body-tilt aircraft's airframe, rotors, and other systems.

Table 1.1: Local Delivery Mission Specification - Residential and Commercial

#	Segment	Time (min)	Range (km)	Final Altitude (m)	Airspeed	Power Available Limit
1	Load package(s)	5	-	1200	-	
2	Warmup	5	-	1200	-	Ground Idle
3	Takeoff HOGE	2	-	1200	-	95% Maximum Rated Power
4	Climb	-	Note 4	1350	Best Climb	100% Maximum Continuous Power
5	Cruise	-	50	1350	Note 5	100% Maximum Continuous Power
6	Descent	-	Note 4	1200	-	100% Maximum Continuous Power
7	Land HOGE	1	-	1200	-	95% Maximum Rated Power
8	Unload Package(s)	Note 8	-	1200	-	- / -
9	Takeoff HOGE	1	-	1200	-	95% Maximum Rated Power
10	Climb	-	Note 4	1350	Best Climb	100% Maximum Continuous Power
11	Cruise	-	50	1350	Note 5	100% Maximum Continuous Power
12	Descent	-	Note 4	1200	-	100% Maximum Continuous Power
13	Land HOGE	1	-	1200	-	95% Maximum Rated Power
14	Reserve	20	-	1350	Best Endurance	100% Maximum Continuous Power

Notes:

1. Design payload 50 kg (W_{pl} = 50 kg)
2. Payload dimensions: 70 cm x 70 cm x 70 cm and 140 cm x 50 cm x 50 cm
3. Block Time = 28 min to end of segment 8 or faster
4. Climb and descent distances credited to cruise range reuirement.
5. Cruise speed is greater of best range speed or airspeed required to meet package delivery window and constrained to continuous power rating.
6. Ambient temperature for all segments = ISA+20C
7. Flight shall be operated at 150 m above ground level (AGL)
8. Cargo unloading method and time requirement determined by proposer with goals to ensure safety while meeting the delivery window and maximizing operational flexibility and customer experience.

From Table 1.1, the mission profile for the local delivery mission has been created and is shown Figure 1.1. Again, Table 1.2 was taken and modified from the RFP and is shown alongside Figure 1.2, its mission profile.

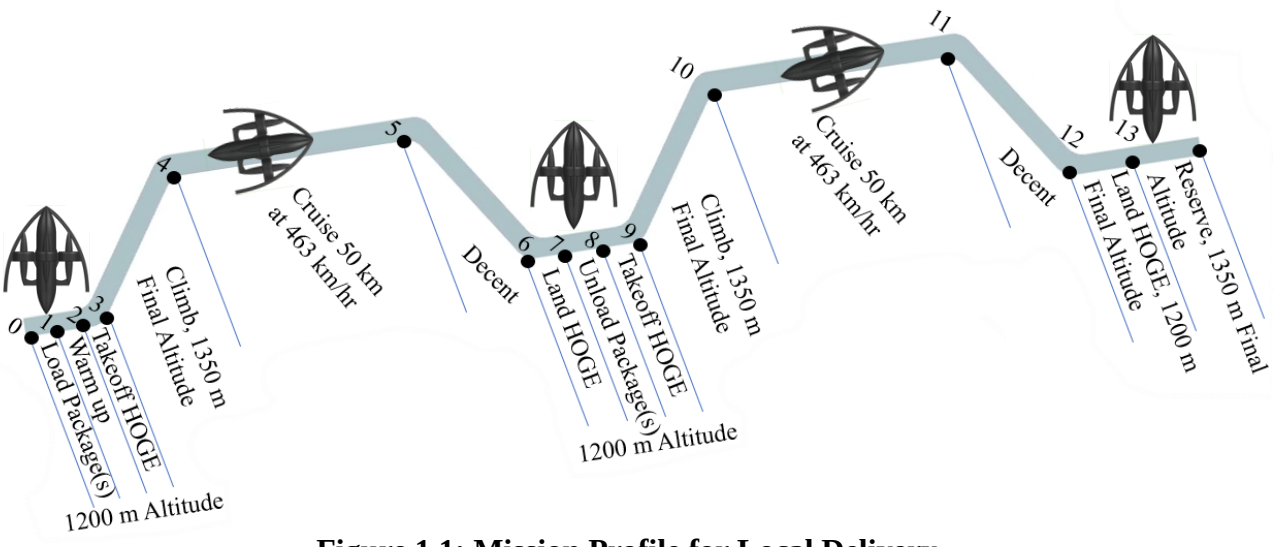

Figure 1.1: Mission Profile for Local Delivery

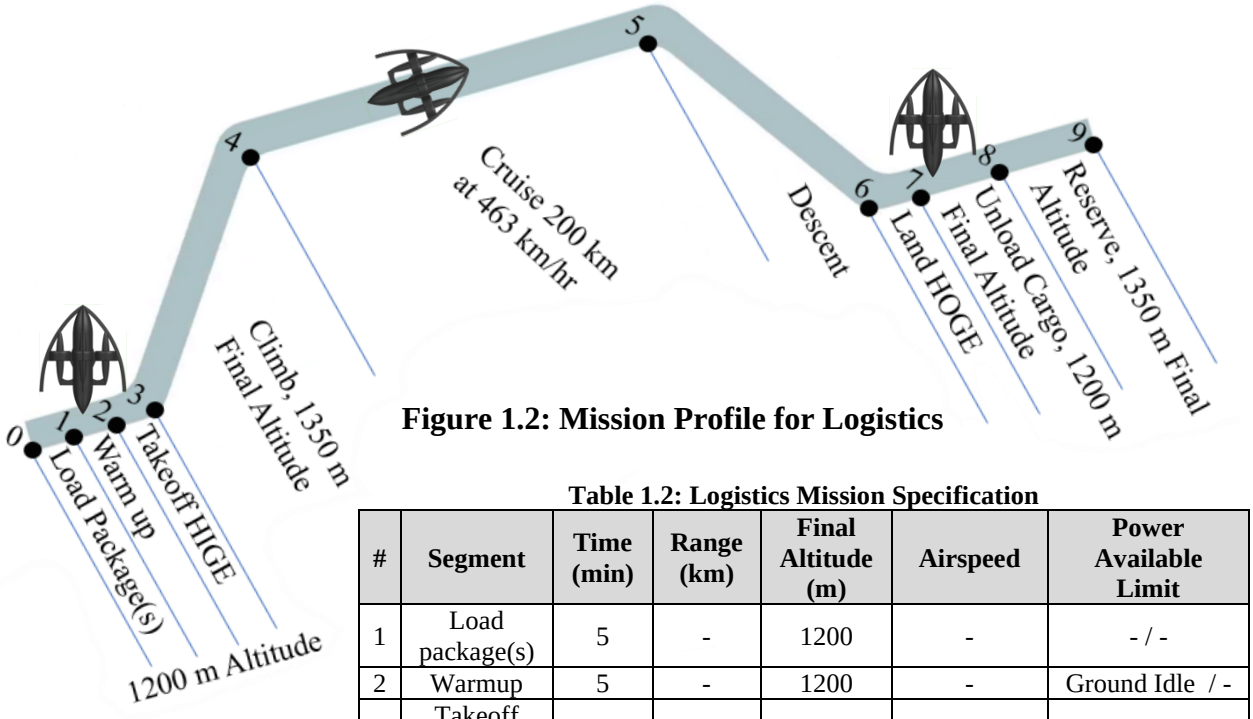

Figure 1.2: Mission Profile for Logistics

Table 1.2: Logistics Mission Specification

#	Segment	Time (min)	Range (km)	Final Altitude (m)	Airspeed	Power Available Limit
1	Load package(s)	5	-	1200	-	- / -
2	Warmup	5	-	1200	-	Ground Idle / -
3	Takeoff HIGE	2	-	1200	-	95% MPR
4	Climb	-	Note 4	1350	Best Climb	100% MCP
5	Cruise	-	200	1350	Note 5	100% MCP
6	Descent	-	Note 4	1200	-	100% MCP
7	Land HOGE	1	-	1200	-	95% MRP
8	Unload Cargo	Note 8	-	1200	-	- / -
9	Reserve	20	-	1350	Best E	95% MRP

Notes:

1. Design payload 50 kg (W_{pl} = 50 kg)
2. Payload dimensions: 70 cm x 70 cm x 70 cm and 140 cm x 50 cm x 50 cm
3. Block Time = 75 min to end of segment 8 or faster
4. Design payload 50 kg (W_{pl} = 50 kg)
5. Payload dimensions: 70 cm x 70 cm x 70 cm and 140 cm x 50 cm x 50 cm
6. Block Time = 75 min to end of segment 8 or faster
7. Climb and descent distances credited to cruise range requirement.
8. Cruise speed is greater of best range speed or airspeed required to meet package delivery window and constrained to continuous power rating.
9. Ambient temperature for all segments = ISA+20C
10. Flight shall be operated at 150 m above ground level (AGL)
11. Cargo unloading method and time requirement determined by proposer with goals to ensure safety while meeting the delivery window and maximizing operational flexibility and customer experience.

Table 1.3: Other Notable Specifications (Ref. 2)

#	Specification	
1	The vehicle operational size shall be less than or equal to:	
	Threshold: 6.1m x 6.1m (20' x 20')	Objective: 4.6m x 4.6m (15' x 15')
2	The Powerplant is not specified. Proposals shall elaborate on the trades leading to the powerplant(s) and energy storage system(s) selection.	
3	System shall be autonomous. An operator "on" the loop shall be considered. The operator would be physically located at a remote site to monitor status and act by exception to machine decisions.	
4	System features, such as obstacle sensing technologies and all technologies required for autonomous flight shall be described and SWaP (space, weight and power consumption estimated).	
5	Delivery site can be assumed to be 15.25m x 15.25m (50' x 50') of flat, clear space	
6	Vehicle shall be equipped with sensors to enable obstacle detection in the vicinity delivery site.	
7	Design and/or operational concepts to minimize risk to people, animals, etc. in vicinity of the vehicle.	
8	Payload handling is of primary concern — the design and/or operational concepts shall emphasize convenience as well as rapid loading/unloading. The payload shall be autonomously released from the vehicle.	
9	Emergency landings not covered by other design requirements in which the vehicle may land on an unprepared surface should be discussed, including safety of people/animals on the ground	
10	Vehicle configuration features like rotor height or shrouds, system features like warning alarms or lights, and infrastructure features like fenced, local landing sites that protect people/customers should be discussed.	
11	The vehicle cannot be refueled/recharged at the delivery site.	

2. HISTORICAL REVIEW AND COMPETITION IN THE MARKET, COMPARISON OF CONCEPTS OF OPERATION

2.1 HISTORICAL REVIEW

The creation of unmanned aerial vehicles began shortly after the advent of the first manned airplanes. Uninhabited vehicles have the distinct advantage of not endangering a pilot, so the demand for research into these designs ballooned during the first world war. Elmer Sperry, an inventor who specialized in gyroscopes, together with Peter Hewitt, created the Hewitt-Sperry Automatic Airplane, one of the first pilotless aircraft. This design and its later successors functioned more like a rudimentary cruise missile but did demonstrate that unmanned aircraft could still nonetheless be controlled without an onboard presence.

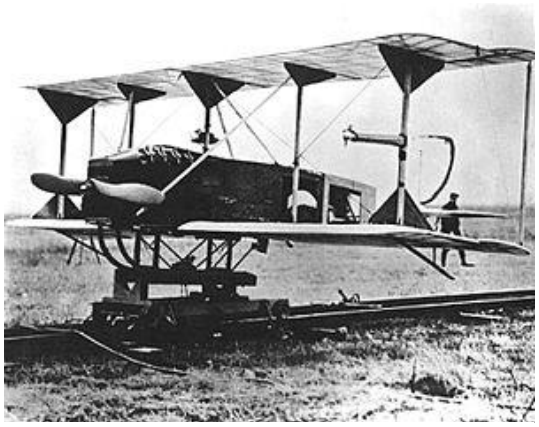

Figure 2.1: The Hewitt-Sperry Automatic Airplane was one of the first unmanned aircraft. (Ref. 3)

For many years, UAVs remained a tool used primarily for war. However, as designs and control methods improved, so did the capabilities of drones. By the turn of the century 21st century drones had entered the public consciousness and what followed was a rapid growth of new applications for the civilian market. In the past twenty years UAVs have been used for a wide variety of programs; from remote sensing of artic ice sheets to border patrol and local law enforcement. A large hobby market also developed in the past decade where mass produced self-controlled toy drones became common place. Recently more corporations are exploring the option of employing UAVs as delivery systems as they can provide better flexibility and convenience over conventional methods. Similar considerations also apply to medical supplies delivery. Often deliveries must be made either at a rapid pace, and/or to an area affected by a large-scale disaster, which are both obstacles that can be difficult for ground vehicles to manage. While manned aircraft such as helicopters can provide this, they are expensive and require highly trained pilots to operate. Unmanned delivery drones can solve both problems and have greater accessibility, which leads to more saved lives.

2.2 COMPETITION IN MARKET

Figure 2.2: The md4-3000 heavy-lifting drone (Ref. 4)

Today the market is inundated with a wide variety of unmanned aerial vehicle concepts. These designs usually fulfill one of two purposes: delivery of relativity light weight cargo, or low passenger count transport. Because the mission specification calls for a design cargo weight target between these two concepts, examples from both will be discussed. Finally, mention will be given to repurposed extant designs.

Small package delivery is the playground of large multinational corporations. These companies have the resources to develop new technologies and the consumer base to market them to. Amazon has been

researching autonomous delivery drones since 2013. While the final design has still not been revealed, Amazon claims the ability to deliver packages of up to 2.25 kg to any location in 30 minutes within a 16 km radius of an Amazon fulfillment center. Currently publicized designs include a standard configuration quadcopter, a tilt wing drone, and a nine bladed vertical takeoff airplane. As the aircraft can carry less than 5% of the weight laid out in the mission specification; it is not a serious threat to this report's design. Other options include workhorse drones like the md4-3000, designed to carry out tasks like terrain mapping and have a useable payload of 5 kg. Still, most existing small sized designs fall far short of the weight and distance requirements provided by the mission specification. The next obvious market competitors therefore lie in autonomous air taxi concepts meant to carry passengers. To be competitive versus cars, trains, and existing aircraft these designs must carry larger weights at higher speeds for longer distances.

Figure 2.3: A prototype of the Volocopter 2X (Ref. 5)

One of such aircraft in the development stage is the Volocopter 2X, which resembles a traditional helicopter setup with 18 individual rotors. This design has 190 kg of useful weight, significantly more than needed for the specification. But because of this the range is only 27 km, far too short for the mission's needs. Other air taxi concepts are tiltwing, like the Airbus Vahana, or tilt rotor, like the Lilium Jet. However, these designs are limited by their electric motors and cannot go the speeds and distances required by the mission specification.

The final concepts to be discussed are unmanned helicopters. Designs such as the remote-controlled Yamaha R-MAX are proven and FAA certified, and could feasibly meet the mission specifications once converted to autonomous control. However, such helicopters were not designed for explicitly this mission, and thus have significant drawbacks in terms of efficiency, speed, and ground safety.

In short, most of the currently public unmanned autonomous delivery aircraft do not fit the mission specification for this report. They are either small sized delivery drones that fail to reach the range and weight requirements, or oversized air taxis running on weak batteries, or helicopter-based systems that were not designed with this type of mission in mind. There are many good useable design elements in these concepts, but they must be applied at different scales to meet the mission specification.

Figure 2.4: The Yamaha R-MAX helicopter (Ref. 6)

2.3 COMPARISON OF CONCEPTS OF OPERATION

Vertical takeoff and landing aircraft can be generally categorized into one of two types. The first of these is a traditional helicopter-like design. Popular in package delivery, these concepts typically feature four or more top mounted rotors that efficiently lift the aircraft with the smallest amount

of power. However, this design suffers from low horizontal travel speeds. This can be improved by using a compound helicopter design, which adds a pusher prop to increase top speeds. The main benefit of these designs beyond vertical efficiency is the ability to hover in place for extended periods of time, helpful for difficult takeoff or landing environments. The other category features a variety of transitioning aircraft, which take off vertically but transition to horizontal flight for cruise. The basest of this type is a tilt rotor concept. Here the aircraft takes off and lands the same as a helicopter design, but transitions to a propeller driven aircraft for horizontal travel. This trades some vertical efficiency for horizontal speed and range. This concept can be improved by tilting the entire wing instead of just the rotors, again improving horizontal travel at the cost of vertical efficiency. Finally, there is the tilt-body design. This allows the entire body of the aircraft to transition into lateral flight once the desired elevation is reached. This concept makes the most sense for vertical takeoff and landing aircraft that must also travel long distances quickly, as there is the least trade off in horizontal speed. The concepts of operation for these two main categories of helicopter or transition-based flight are shown in the Figures below.

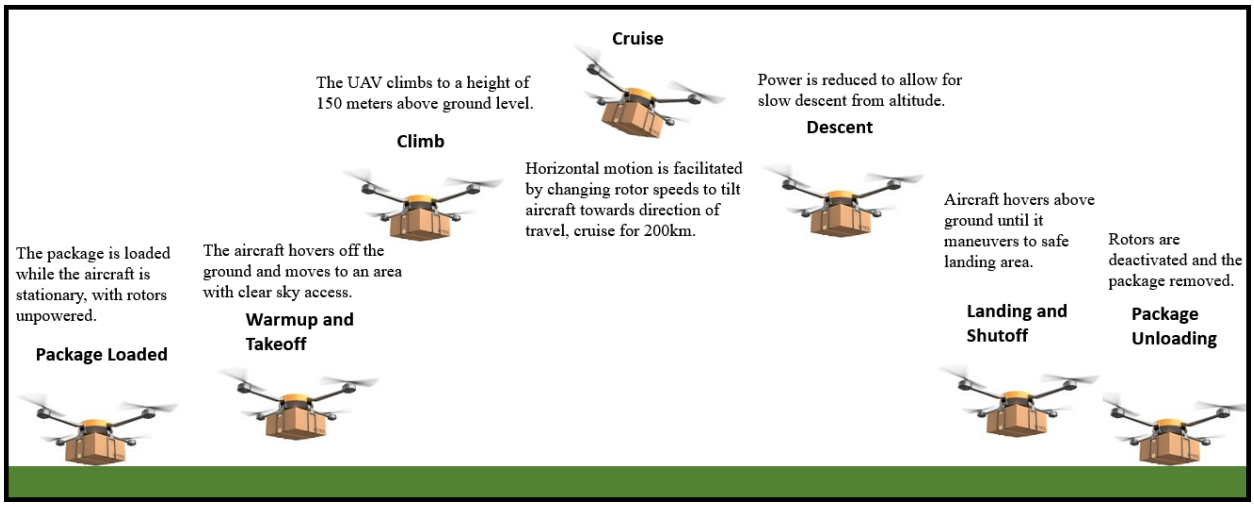

Figure 2.5: Concept of Operation for a Quadcopter Design

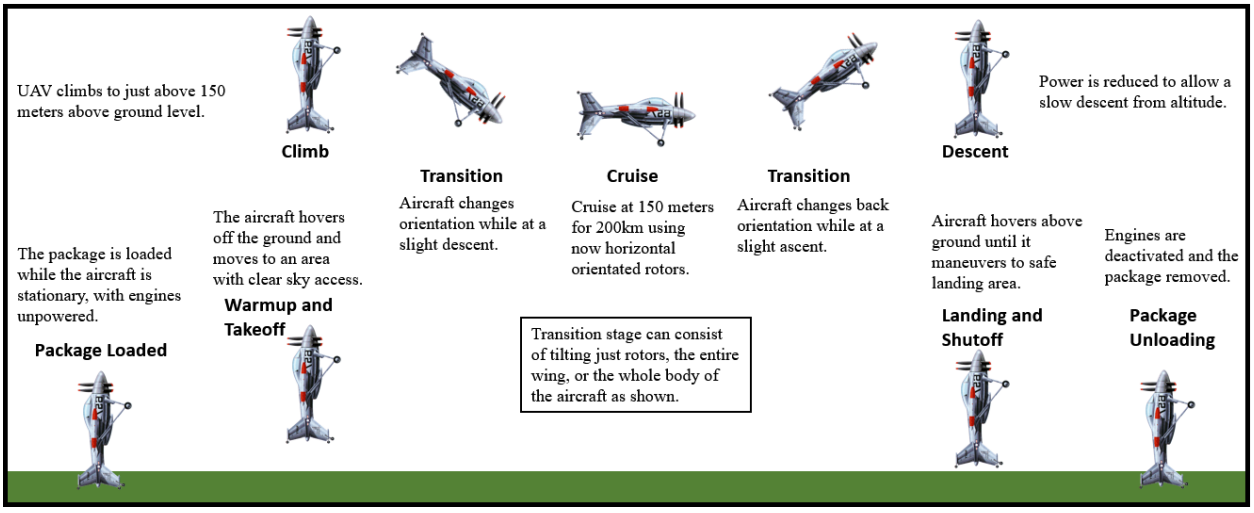

Figure 2.6: Concept of Operation for a Convertible Design

3. OPTIMIZATION FUNCTION, ECONOMICS MODEL, LIFE-CYCLE COST MINIMIZATION AND WEIGHTS ESTABLISHMENT

3.1 DESIGN OPTIMIZATION FUNCTION

Table 3.1 lists design considerations that should be met, but are not specified by the RFP.

Table 3.1: Ancillary Design Considerations

#	Requirement
1	Must be able to fly in 10^{-6} atmospherics under Mil-F-8785c
2	Must meet FAR-29 OEI conditions
3	No child or adult human body part may come in contact with any rotating component-catastrophic failure
4	Controlled landing w/o damage to a/c beyond acceptable maintenance limits NB: Define "Acceptable Maint. Lims"
5	Must be flightworthy, controllable, and stable following cable strike at full forward speed
6	Must be flightworthy, controllable, and stable following a wall strike at up to 15 g's
7	Must be able to survive urban gust loads up to 10^{-6} atmospherics
8	Must be ADS-B compliant
9	Minimize noise radiated towards ground during cruise, but generate at least 90dBA upon landing
10	Minimize acquisition cost
11	Minimize direct operating costs
12	Insignificant Aircraft CG Excursions

Table 3.2 shows the requirement weighting functions gathered from the RFP. Note that these functions are weighted binarily.

Table 3.2: Requirement Weighting Functions

#	Requirement
1	"Acceptably Safe" (see SAE ARP4761, FAR part 21 NB "Acceptably Safe" needs to be defined)
2	Autonomous landing w/in 15.25m x 15.25m flat, clear space
3	Fifteen minutes of safe flight after a non-catastrophic failure
4	Controlled landing w/o damage to a/c beyond acceptable maintenance limits NB: Define "Acceptable Maint. Lims"
5	Assessment of unprepared landing site by a/c
6	No reconfiguration allowed between missions
7	Cognizance of FAA class airspace
8	Collision avoidance NB: to what level of precision?
9	Flight over inhabited areas NB: FAA clearance needed
10	No recharging or refueling at delivery site
11	VFR flight day and night operations
12	6.1m x 6.1m NB: 3rd dimension missing
13	Fully autonomous flight with operator in the loop
14	Autonomous release of payload from vehicle
15	Must be capable of being FAA certified
16	W_{pl} = 50kg (internal or external)
17	Max PL dimensions: 70 x 70 x 70cm + 50 x 50 x 140cm
18	Block time <75min to 200km(x1), <28min to 50km(x2)

Table 3.2 Continued	
19	hcr = 150m AGL
20	HIGE 2min at 1200m ISA + 20C
21	Climb to 1350m ISA + 20C at Vbc, max. continuous power, NB: time to climb unspecified
22	Cruise 200km or 50km, 1350m ISA + 20C at V_{dash}, NB: range credit for ascent & descent, max. cont. power
23	HOGE 1 min. ISA + 20C @ 1200m
24	Land @ 1200m ISA + 20C
25	Loiter 20m @ 1200m, ISA + 20C V_{be}

From the RFP, three objective weighting functions have been derived (Eq. 3.1 – Eq. 3.3). Said objective weighting functions are as follows:

O_1: Vehicle Operational Size (VOS)
VOS = 6.1m when OF = 0, & VOS = 4.6m when OF = 1

$$OF_1 = OF_{size} = 1 - \frac{VOS - 4.6m}{6.1 - 4.6m} = 4.07 - \frac{2}{3}VOS \quad \text{(Eq. 3.1)}$$

O_2: Safety highly weighted OF = 0 when $P_{fatality}$ = medical helicopter = $2*10^{-5}$, & OF = 1 when $P_{fatality}$ = FAR-25 = 10^{-9}

$$OF_2 = OF_{safety} = \frac{ftlexp - 5}{4} = \frac{1}{4}ftlexp - \frac{5}{4} \quad \text{where } P_{fatality} = 10^{-ftlexp} \quad \text{(Eq. 3.2)}$$

(ftlexp = Fatal Experience)

O_3: Mission Productivity = $(W_{pl} * V_{dash})/W_{to}$
FAA restricts $V_{flt} \leq$ 250kts at h < 10,000 ft, W_{pl}/W_{tomax} = 0.45 (at 200km mission) $OF_{Mission\ productivity} = OF_{dash} * OF_{Wpl/Wto}$

$$OF_3 = OF_{prod} = OF_{speed}OF_{PLfract} = \left(\frac{V_{flt}}{164} - 0.52\right)\left(5.10\frac{W_{PL}}{W_{TO}} - 0.275\right) \quad \text{(Eq. 3.3)}$$

A general optimization can be used for design downselection and is shown by Eq. 3.4.

$$General\ Optimization\ Function = GOF = \prod_{1}^{l} R_i \left(\frac{1}{m}\sum_{1}^{m} O_j + \frac{1}{nROWF}\sum_{\mathbf{1}}^{n} A\boldsymbol{O}_k\right) \quad \text{(Eq. 3.4)}$$

3.2 ECONOMICS MODEL

To develop a basic economics model, research on various VTOL design categories is necessary and provided in Table 3.3 and Table 3.4.

Table 3.3: Quadcopter and Hexacopter Drone Data

#	Aircraft	W_{to} (kg)	V_{max} (kph)	E (min)	Price ($)	W_{pl} (kg)
1	PHANTOM 4 RTK (Ref. 7 & 8)	1.4	58	30	6500	-
2	Yuneec H520 RTK (Ref. 9 & 10)	1.6	61	25	3200	-
3	MATRICE 200 Series (Ref. 11 & 12)	6.1	83	24	10000	2.3
4	MATRICE 600 Pro (Ref. 13 & 14)	16	65	16	6600	6.0

Table 3.4: Drone Copter Data

#	Aircraft	W_{to} (kg)	V_{max} (kph)	E (min)	Price ($)	W_{pl} (kg)
1	Yamaha R-max (Ref. 15 &16)	94	74	60	80000-120000	31
2	Yamaha Fazor (Ref. 17)	150	150	120	-	70
3	Yamaha Fazor R (Ref. 17)	110	72	100	130000	35

3.3 LIFE-CYCLE COST MINIMIZATION

Figure 3.2 shows cost of aircraft acquisition versus aircraft type. From Table 3.3 and Table 3.4 a relationship between VTOL payload and Aircraft cost has been provided in Figure 3.3.

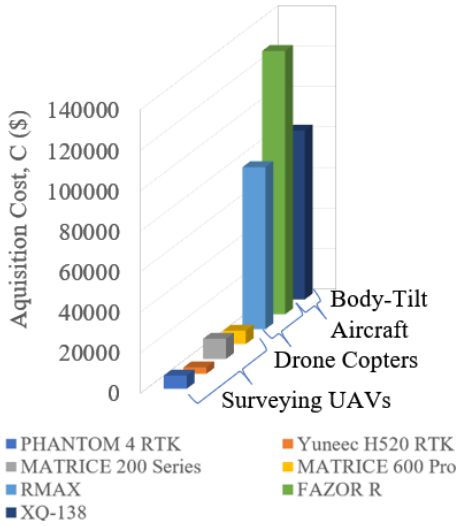

Figure 3.2: VTOL Aircraft Type as a Function of Acquisition Cost

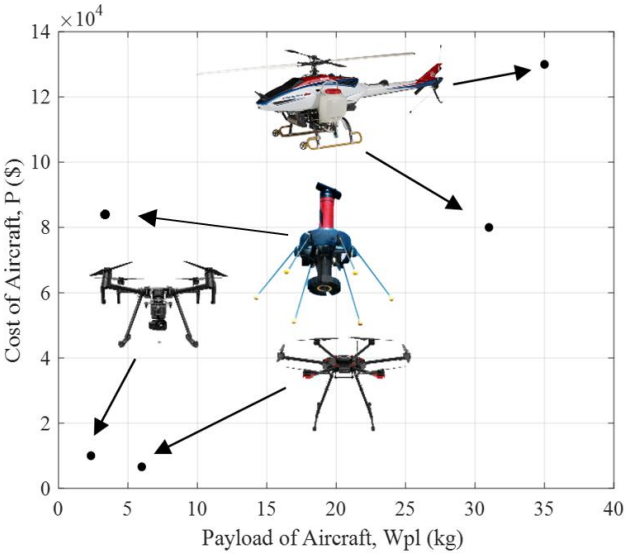

Figure 3.3: Basic Cost Estimation for VTOL Aircraft

According to FEHR PEERS, a transportation planning and engineering firm (Ref. 18), "Typical UPS and FedEx ground delivery may cost upward of $6 for delivery from a local distribution warehouse, drone delivery could be as cheap as $0.05 per mile with delivery in about 30 minutes." This information provides a good foundation for the cost of operation of personal surveying drones and delivery drones. Information around cost of operation of other drone categories is more obscure but is likely in line with traditional small aircraft.

In addition to operating costs, maintenance will also be necessary to consider for minimizing life-cycle costs. One estimation of maintenance has been provided for a twin boom drone by Washington State University (Ref. 19). They estimated that for their small UAS, "$500 every 200 hours."

4. STATISTICAL TIME AND MARKET PREDICTIVE ENGINEERING DESIGN (STAMPED) ANALYISIS OF SIMILAR UAVS

In this section, UAVs which have demonstrated some ability to complete the mission specification are compared. From important characteristics of these aircraft conclusions can be drawn about the general performance figures for an aircraft in this size and weight class.

Table 4.1 Characteristics of Similar VTOL Aircraft

Name	Type	Year	Range (km)	Payload (kg)	Empty Weight (kg)	Takeoff Weight (kg)	Cruise (km/h)	Engines	We/Wto
Lilium Jet	Tilt Rotor	2019	300	200	440	640	300	32	0.688
Volocopter VoloCity	Multicopter	2019	35	200	700	900	110	18	0.778
Vertical Aerospace VA-1X	Tilt Rotor	2020	161	450	~	~	241	8	~
Yamaha R-MAX	Helicopter	1997	74	31	64	94	74	1	0.681
Yamaha Fazer	Helicopter	2007	300	70	80	150	150	1	0.533
Yamaha Fazer R	Helicopter	2016	90	35	71	110	72	1	0.645

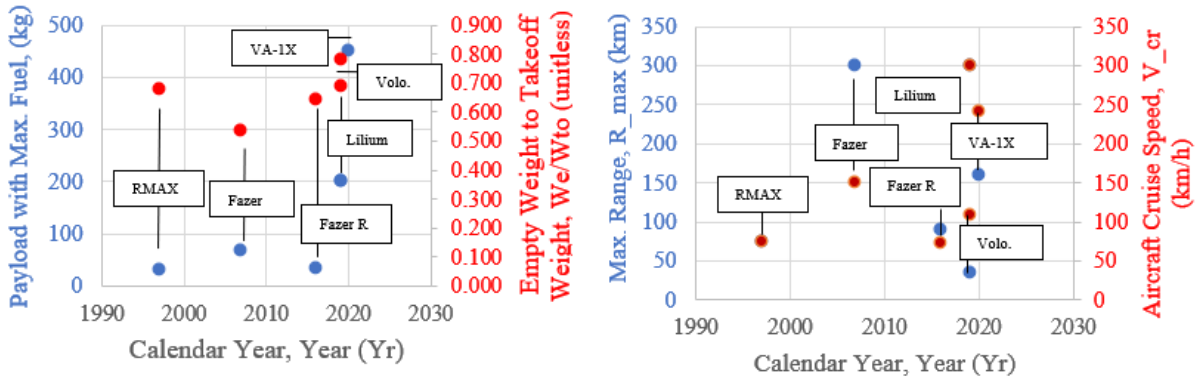

Figure 4.1 STAMPED Time Trends for W_e/W_{TO}, Maximum Range, Payload, and Cruise Speed

As there are not enough data points to make a trendline statically significant, conclusions will instead be drawn from averages. Most important is the $\frac{W_e}{W_{TO}}$ ratio, which determines how much of the aircraft weight must be split between structure, payload, and fuel. From this data set:

- The average Cruise Speed is 157 km/h
- The average Takeoff Weight is 379 kg
- The average Range is 160 km
- The average $\frac{W_e}{W_{TO}}$ is 0.63

5. WEIGHT SIZING CODE GENERATION

The method described by Roskam in Airplane Design Part I (Ref. 20) will be used for preliminary weight sizing. To do this, assumptions are made about the fuel burn rates at different stages of the mission profile, with those for the Warmup, Takeoff, Climb, Descent, and Land coming from the homebuilt assumption in Table 2.1 of Roskam's textbook. For the cruise and endurance legs, Breguet's Range and Endurance equations were used, shown below.

$$R_{cr} = \left(\frac{V}{c_j}\right)_{cr} \cdot \left(\frac{L}{D}\right)_{cr} \cdot \ln\left(\frac{W_4}{W_5}\right) \qquad \text{(Eq. 5.1)}$$

$$R_{cr} = \left(\frac{V}{c_j}\right)_{cr} \cdot \left(\frac{L}{D}\right)_{cr} \cdot \ln\left(\frac{W_4}{W_5}\right) \qquad \text{(Eq. 5.1)}$$

With these equations solved for the mission specification range and endurance, and with values for $\frac{L}{D}$, c_p and η_p estimated from Roskam's Table 2.2, the fuel burn ratios for the remaining stages could be found. Using Eq. 5.1 and 5.2, these weight ratios combine to produce an estimate for the required fuel weight, W_F.

Table 5.1: Logistic Mission Fuel Fractions

W_2/W_1	W_3/W_2	W_4/W_3	W_5/W_4	W_6/W_5	W_7/W_6	W_8/W_7
0.995	0.99	0.98	0.94	0.95	0.98	0.99

$$M_{ff} = \frac{W_2}{W_{TO}}\frac{W_3}{W_2}\frac{W_4}{W_3}\frac{W_5}{W_4}\frac{W_6}{W_5}\frac{W_7}{W_6} \qquad \text{(Eq. 5.2)} \qquad W_F = (1 - M_{ff})W_{TO} \qquad \text{(Eq. 5.3)}$$

From there, a tentative estimate about the aircraft empty weight can be made by subtracting the weight of the fuel from the takeoff weight guess. Next, that tentative empty weight estimate is compared to the value gotten by multiplying the takeoff weight guess with the STAMPED average value for $\frac{W_e}{W_{TO}}$. The takeoff weight guess was then increased through iteration until the two empty weight values were within 0.5% of each other.

- W_{TO} = 221 kg or 488 lb
- W_e = 140 kg or 308 lb
- W_F = 32 kg or 70.6 lb

6. WING, POWERPLANT, & DASH-SPEED PRELIMINARY SIZING

To estimate drag polar (which is needed for dash sizing) it is necessary to acquire the wetted area of the design and solve for parasite area. This can be done using Eq. 6.1 from Ref. 20.

$$\log_{10} f = -2.4 + \log_{10} S_{wet} \qquad \text{(Eq. 6.1)}$$

Using a basic CAD model, an estimation for the wetted area was found to be 831 ft^2. From Eq. 6.2 (Ref. 20) the zero-lift drag coefficient can be estimated.

$$C_{D_0} = \frac{f}{S} = \frac{3.32\ ft^2}{19.0\ ft^2} = 0.175 \qquad \text{(Eq. 6.2)}$$

The Aspect Ratio is defined by Eq. 6.3, where geometric values were taken from the convertible-tilt aircraft CAD model.

$$AR = \frac{b_{duct}}{c_{duct}} = \frac{5038\ mm}{350\ mm} = 14.4 \qquad \text{(Eq. 6.3)}$$

Using Table 3.6 from Ref. 20, the change in zero-lift drag coefficient due to landing gear can be estimated as 0.15. Thus, Equations 6.3 and 6.4 are the design's drag polar.

$$C_{D,clean} = C_{D_0} + \frac{{C_L}^2}{\pi ARe} = 0.175 + 0.0233{C_L}^2 \qquad \text{(Eq. 6.4)}$$

$$C_{D,Landing\ Gear} = C_{D_0} + \frac{{C_L}^2}{\pi ARe} = 0.19 + 0.0233{C_L}^2 \qquad \text{(Eq. 6.5)}$$

Eq. 6.6 can then be used to determine the minimum shaft power required necessary to meet FAR 29.67 OEI conditions.

$$P = \frac{T^{3/2}}{FM\sqrt{2\rho A}} = \frac{(493\ lb)^{3/2}}{0.68\sqrt{2(0.002045\ \frac{lbf - s}{ft^4})(2\pi(3.5\ ft)^2\ )}} \frac{1\ hp}{550\ \frac{ft - lbf}{s}} = 52.1\ hp \qquad \text{(Eq. 6.6)}$$

Eq. 6.7 can be used to determine the minimum shaft power required to account for a one in a million-gust encounter maneuver load.

Eq. 6.8 can be used to transpose the minimum shaft power required to sea level.

$$P_{sgust} = 1.5P_s = 65.1\ hp \qquad \text{(Eq. 6.7)}$$

Dividing Eq. 6.8 by two solves for the power required per engine (38 hp) under the proposed sizing conditions. Thus, the total power needed to satisfy FAR 29.67 and 10^{-6} atmospheric conditions transposed at sea level is roughly 152 hp.

$$P_{SL} = \frac{P_{alt}}{\sigma} = \frac{65.1\ hp}{0.86} = 75.7\ hp \qquad \text{(Eq. 6.8)}$$

Using Eq. 6.9, the power-loading as a function of the wing loading can be plotted with a sweep of dash speeds.

$$\frac{W}{P_s} = \frac{\eta_p}{\left(\frac{\bar{q}C_{D_o}}{W/_S} + \frac{W/_S}{\bar{q}\pi ARe}\right)V} \qquad \text{(Eq. 6.9)}$$

7. CONFIGURATION MATRIX AND DOWNSELECTION

As discussed, there are several different configurations that are common in the VTOL market and which could be adapted to work for this mission specification. These configurations range from traditional quadcopters and helicopters to tiltrotor and tiltwing designs. A sample of each broad type of configuration are shown below, alongside the benefits and drawbacks of that approach.

Pros:

- Simple to manufacture
- Easy to certify
- Proven design

Cons:

OF = 1.13

- Slow top speed
- Many extant similar designs
- Wire strike

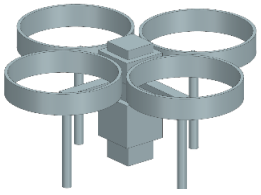

Configuration 1

Pros:

- Simple to manufacture
- Easy to certify
- Proven design

Cons:

OF = 0.92

- Slow top speed
- Many extant similar designs
- Open blades
- Wire strike

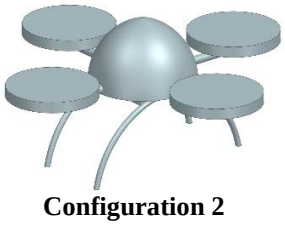

Configuration 2

Pros:

- Flight safety
- Proven design

Cons:

OF = 0, Req. no. 18 Failed

- Slow top speed
- Open blades
- Wire strike

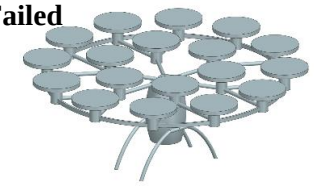

Configuration 3

Pros:

- Hover efficiency
- Easy to certify
- Public acceptance

Cons:

OF = 0.86

- Many extant similar designs
- Open blades
- Wire strike

Configuration 4

Pros:

- Long range flight
- High top speeds
- Conventional arrangement

Cons:

OF = 1.22

- Open blades
- Weight in back
- Hover efficiency
- Wire strike

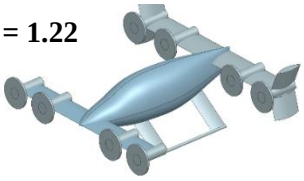

Configuration 5

Pros:

- Long range flight
- Ground mobility
- Closed blades

Cons:

OF = 1.51

- Hover efficiency
- Weight in back
- Engine positioning
- Wire strike

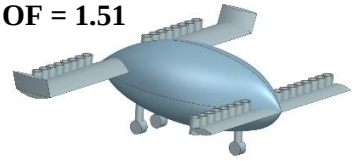

Configuration 6

Pros:

- High top speeds
- Closed blades

Cons:

OF = 1.02

- Public acceptance
- Inherently unstable
- Hard to control
- Gust loads

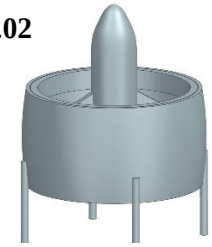

Configuration 7

Pros:

- Compatible with ballistic chutes
- Building strike resistant
- Body parts cannot touch blades
- Cable strike resistant
- Gust resistant

Cons:

OF = 1.68

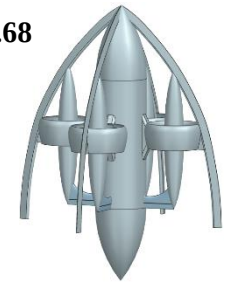

Configuration 8

One issue with nearly every configuration is the possibility of human contact with spinning rotors, which is a real danger with fully autonomous systems. If even one person where to be

injured by a medical VTOL designed to save lives, the whole program could be shut down due to safety concerns. Thus, from these configurations, the clear standout for this mission's specification is the body tilt design. The desired aircraft must travel long distances at high speeds while remaining controllable and safe to civilians. Configuration 8 satisfies these conditions better than any of the other more conventional designs, as seen in its highest optimization function score.

8. FUSELAGE LAYOUT DESIGN

The first major component of the aircraft to be designed is the fuselage. The fuselage is the core of the design and must serve as the main housing for the payload, the payload delivery system, and the avionics that enable the aircraft to fly autonomously. Each of these components and their effect on the design are discussed below.

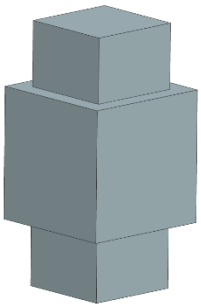

Figure 8.1: Payload Shape

The sizing of the fuselage is determined largely by the mission packaged specified in the RFP of the two shapes of dimensions 50cm by 50cm by 140cm and 70cm by 70cm by 70cm. To reduce the volume of the cargo bay where the packages are stored as much as possible, the two rectangles are co-located so they share the same center of gravity, producing the shape shown in Figure 8.1.

Because a body convertible concept of operation has been chosen for this design it is important that the overall center of gravity of the aircraft is able to stay as close as possible to the design position, even if the weight of the cargo is not always the maximum 50kg or has its center of gravity at the center of volume. To address this the cargo bay is designed to be moved up or down the length of the fuselage up to 30cm either direction, allowing the payload center of gravity to be moved to the right position that keeps the aircraft center of gravity correctly placed. This system, utilizing small inflatable inner airbags, adds an additional length of 60cm to the fuselage, which main section must now be at least as large as Figure 8.2.

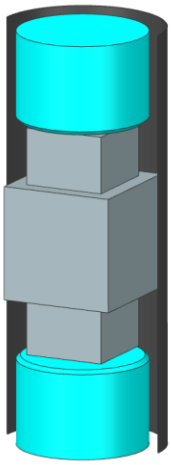

Figure 8.2: Base Fuselage Shape

The next thing to consider is payload delivery. The most sensible place to load and unload the payload is from a payload door near the bottom of the aircraft. This way the door can be extended to lie on the ground surface, and the package needs only to be placed on the tray to load the aircraft, as a 50kg weight can be unwieldly for a single person to lift high distances. Once placed, the cargo is then dealt with automatically by the aircraft positioning system until it is ready for delivery at the landing site, and the door automatically opens revealing the package.

Next, the fuselage must accommodate all the onboard avionics that allow for unmanned flight. This includes navigational cameras, receivers, transponders, IMU's, and the autopilot, alongside the batteries which power them and the electrical connections between the systems. As the rear of the fuselage is taken up by the payload positioning and delivery systems, the best available space remaining for the electrical systems is in front of the cargo bay, as part of the fuselage nose. There the components have easy electrical access both down the sides of the fuselage and through the protective arches surrounding the design. The proposed layout of the electrical components is further discussed in Chapter 17.

The overall shape of the fuselage is thus a simple cylindrical shape with a tapered front. By using a tangent ogive shape for the nose, the flow separation is reduced along the surface of the fuselage, as laminar flow is maintained. To stay under the objective dimension of 15 ft, the tail end of the fuselage will be rounded off to sit evenly on the ground surface. The drag issues this

Length = 17.9 ft

Figure 8.4: Full Fuselage Dimensions

causes will be addressed and resolved in Chapter 13. The final dimensioned outer mold line of the fuselage is shown in the Figure 8.3 below. The simple shapes leads to an easy structure of monocoque composite over stringers with a bulkhead between the nose and cargo bay.

Figure 8.4: Basic Arch Shape

One additional component also arose during fuselage design. With the desired speeds of the aircraft being so high, and the height of cruise only 150m AGL, it was decided that the fuselage needed more protection in case of a wire or building strike. By adding four arches along the lengths of the fuselage, acting as overlong canards, a type of roll cage was made around the payload that protects the cargo from direct collisions. These arches additionally provide points for structural integrations of other systems, which will be discussed later.

9. ENGINE INSTALLATION

Choosing the correct propulsion system for the application is an extremely important step in the design of any aircraft. As the RFP did not restrict the type of engine used, it was up to the report authors to determine what propulsion method best fit the design and methodology. The first considered option was electrical motors, as

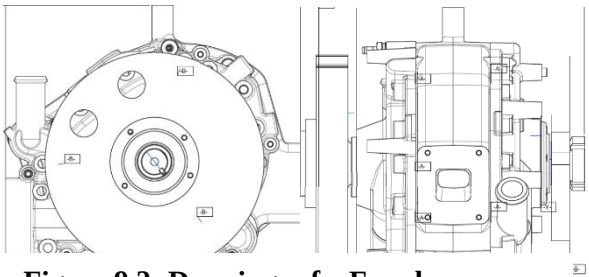

Figure 9.2: Drawings of a Freedom Motors Engine (Ref. 21)

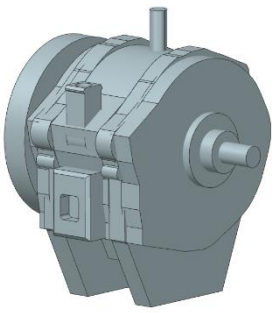

Figure 9.1: Basic CAD of Engine

eVTOL concepts are increasingly popular in the market and have better noise and emission outcomes when compared to traditional fuel-based systems. However, with both the range and speed that the RFP called for, it was determined that the number of electrical motors required to meet the desired targets did not fit with the design concept that could best fulfill the rest of the mission specification. A solution was found by adopting the use of a Wankel based engine. Rotary Wankel engines have fewer moving parts than a traditional engine and are dynamically balanced, which reduces risk of uncontrolled engine vibration in flight. Furthermore, the 4-cycle Rotary RotaPower engine series by Freedom Motors have an excellent power to weight ratio and are particularly fuel efficient when compared to traditional engines. Freedom Motors also offers a wide range of engine sizes, from 20hp up to 150hp varieties, meaning whatever power rating needed for the aircraft can be met. A basic CAD model of a Freedom Motors engine is shown in Figure 9.1, and three-view drawings if Figure 9.2. A table of salient characteristics is provided below.

Table 9.1: Characteristics of the multi-rotor Freedom-Motor 150 series

Displacement	Weight	Fuel System	Cooling	Dimensions	Power	Speed	S.F.C.
300cc	16 kg	Carburetor/EFI	Air	25 x 18 x 18cm	40 hp	6000 rpm	305g/kWh

With an engine type decided on, the next step is the implantation of the propulsion system into the design. Due to the RFP size constraints and nature of a body convertible concept, the obvious implementation method for the engines is a ring wing. Because multiple engines will be needed for both power and safety in case of engine failure, wrapping each engine in a duct that each act as a ring wing, with a Clark YM-18 airfoil, was the converged solution. Ducted fans have two distinct advantages: the reduction of tip losses and the concealing of dangerous moving parts. Furthermore, separating each engine into a "power-pod" assembly allows for axial symmetry throughout the design, drastically simplifying both interior systems design and control of the aircraft. To achieve this symmetry, it was decided that four engines, one in each cardinal direction, was the most elegant solution. In this way the engines could be cross-shafted, further increasing safety during engine failure cases. This layout, in the cross formation, is shown in Figure 9.3. The individual ring wings also have the advantage of excess inner volume that can be used for fuel storage, freeing fuselage space. Each ring contains a self-sealing bladdered fuel tank which keeps the fuel center of gravity consistent despite changes in either fuel volume or body orientation.

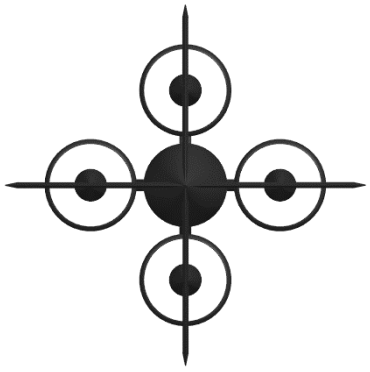

Figure 9.3: Engine Layout Top View

Figure 9.4: Engine Inlet/Duct Assembly

With the positioning and type of engine assembly decided, the next step was to determine the inlet and outlet systems for feeding the engine. As the aircraft is specified to fly at only 150m above ground level, it is imperative that engine noise is reduced to at least an acceptable level. One way to do

this is to increase the volume of the exhaust chamber muffler to help deaden the louder exhaust sounds. To accomplish this, an as large as possible volume was wrapped around the engine, then was shaped to be tangent ogives to cause as little drag as possible. From there, the volume works also as both a large structural competent anchoring the outside arches to the engine assembly, and as a tailboom for the empennage. This structural synergism is combined with the ability of funneling the engine exhaust through the arches, out the back of the aircraft. The design at this stage is shown in Figure 9.4.

The final step in designing the power pod assembly is to connect the engine and exhaust systems to the ring wing. While large stators are the traditional means of connection, the University of Kansas has access to a patent-pending technology known as micro-stators. These fulfill the purposes of regular stators but have several additional desired traits; they both quiet the engine and increase safety. Their advantages will be discussed further in Chapter 21.

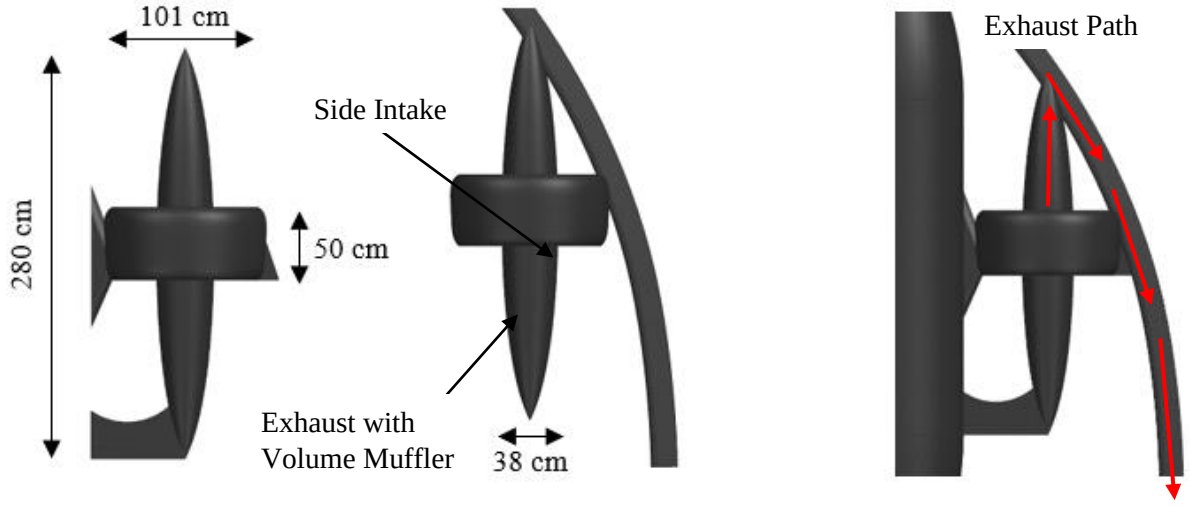

Figure 9.5: CAD of Intake and Exhaust System Integration

10. ROTOR AND WING LAYOUT DESIGNS, IMPLEMENTATION OF BEMT CODE FOR DETAILED ROTOR DESIGN

Determining the precise diameter of the rotor blades is an important step at this stage of the design process. To do so, a Blade Element Momentum Theory code was used to establish the necessary rotor diameters and required shaft power for different potential aircraft takeoff weights. To simply matters, the entire aircraft assembly can be split into four identical partitions that will be analyzed as individual coleopters. The difficulty with this design is the two distinct flight phases the rotors must be efficient in. The first of these is during a hover configuration flight. Here the power required is simply equal to the weight of the aircraft and is independent of rotor size. The second flight mode, horizontal travel after body-tilt, requires significantly more calculations to determine the required thrust at each rotor diameter to reach the objective of a top speed of 250

knots. Using general relationships between rotor diameter and aircraft characteristics, estimates for C_{D_0}, S_{wing}, S_{wet}, $C_{L_{Dash}}$, $C_{D_{Dash}}$, and finally T_{Dash} can be established.

$$C_{D_{Dash}} = C_{D_0} + \frac{{C_{L_{Dash}}}^2}{\pi ARe} = \frac{10^{-2.3979+\log_{10} S_{wet}}}{1.1{D_{rotor}}^2} + \frac{{C_{L_{Dash}}}^2}{1.1\pi} \quad \text{Eq. 10.1}$$

$$S_{wing} = 2 * b_{duct} c_{duct} = 1.1{D_{rotor}}^2 \quad \text{Eq. 10.2}$$

$$T_{Dash} = \frac{1}{2}\rho V^2 C_{D_{Dash}} S_{wing} \quad \text{Eq. 10.3}$$

$$S_{wet} = 4.3{D_{rotor}}^2 \quad \text{Eq. 10.4}$$

$$AR = \frac{b_{duct}}{c_{duct}} = \frac{1.1D_r}{2*(D_r/2)} = 1.1 \quad \text{Eq. 10.5}$$

$$C_{L_{Dash}} = \frac{2W}{\rho V^2 S_{wing}} \quad \text{Eq. 10.6}$$

$$f = 10^{-2.3979+\log_{10} S_{wet}} \quad \text{Eq. 10.7}$$

$$C_{D_0} = \frac{f}{S_{wing}} = \frac{10^{-2.3979+\log_{10} S_{wet}}}{1.1{D_{rotor}}^2} \quad \text{Eq. 10.8}$$

Now with the required thrust value known for each rotor diameter the BEMT code can be used to determine the required shaft power to achieve that thrust. Once a suitable rotor was designed for the dash condition, the rotor $Theta_0$was altered to keep the rotor efficient in hover as well. Calculations were run for rotors between two and seven feet in diameter, for an aircraft with takeoff weights of 400, 500, and 600lb to create sizing curves. The relationship between these curves can be seen in Figure 10.1. Standard atmosphere was used for density calculated at a 5000 ft altitude.

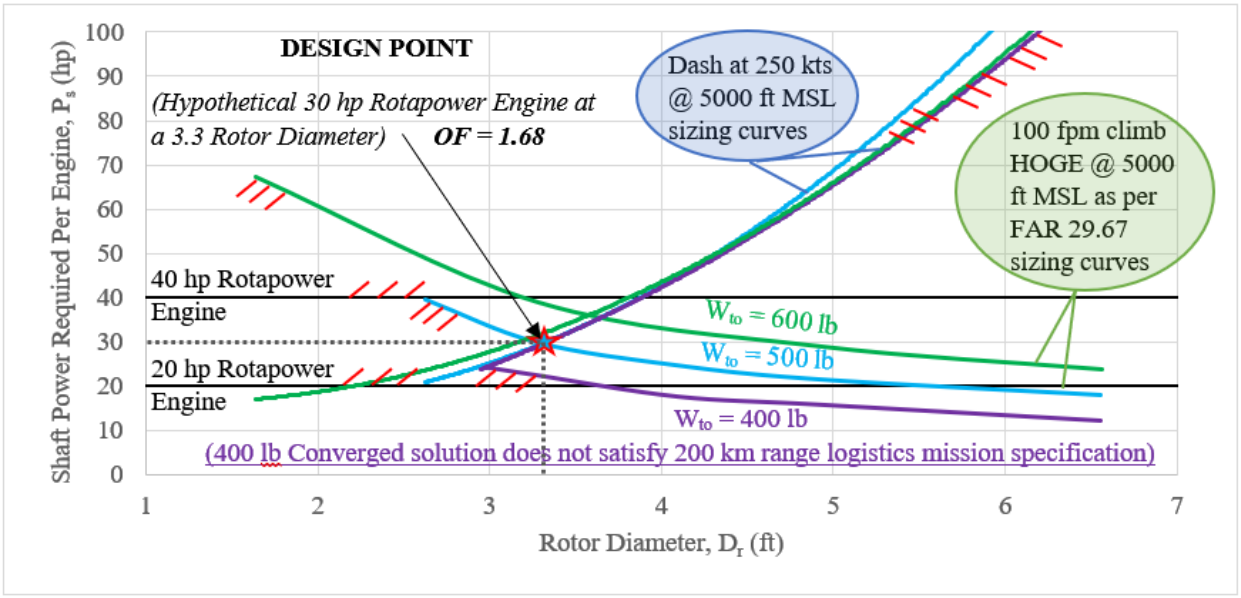

Figure 10.1: Rotor Sizing Chart Generated Using BEMT Results

From the intersections of the hover and dash sizing curves, the following values can be determined:

- At 400lb the converged rotor size is about 3 feet in diameter with a power of ~ 24 hp per power pod;

- At 500lb the converged rotor size is about 3.3 feet in diameter with a power of ~ 30 hp per power pod;
- At 600lb the converged rotor size is about 3.7 feet in diameter with a power of ~ 36 hp per power pod.

The Tables 10.1 and 10.2 below show the defining characteristics of the rotor design for dash and hover at a 500 lb takeoff weight.

Table 10.1: Rotor Characteristics for Dash

Root Chord (mm)	Taper Ratio (~)	$Theta_0$ (deg)	$Theta_1$ (deg)	R Twist exponent (~)	# of blades
50	.9	44.6	65	-0.49	2

Table 10.2: Rotor Characteristics for Hover

Root Chord (mm)	Taper Ratio (~)	$Theta_0$ (deg)	$Theta_1$ (deg)	R Twist exponent (~)	# of blades
50	.9	-15.8	65	-0.49	2

11. EMPENNAGE DESIGN

With the overall configuration of the design mostly complete, the empennage only must function as the control method housing for the aircraft. Because of the structural synergisms shown in previous sections, an obvious place for the controls to be mounted has already arisen between the fuselage end and the muffler volume ends. Here, turning vane flaps have been installed to control the aircraft. As the design is axially symmetrical, these flaps provide all the control needed to perform the inflight operations of transitioning into and out of horizontal flight orientation, maneuvering around ground obstacles while in the vertical orientation, and steering towards the destination and around obstacles during cruise.

To increase safety, each turning flap is outfitted with three flight control servos. Together, any two servos can overpower and rip out a third malfunctioning servo. The flaps are also protected from tail strikes by the outer arches.

An isometric view and planform view of the preliminary turning flap design can be seen in Figure 11.1. A NACA 0012 was used to create the turning flaps. Using the volume coefficient from the XQ-139, the turning flap reference area can be solved for, as seen in Equation 11.1.

$$S_F = \frac{\bar{V}_F S_{wing} \bar{c}}{x_F} = \frac{(.57)\,(11.8\,ft^2)(1.65\,ft)}{4.95\,ft} = 2.24 ft^2 \qquad \text{Eq. 11.1}$$

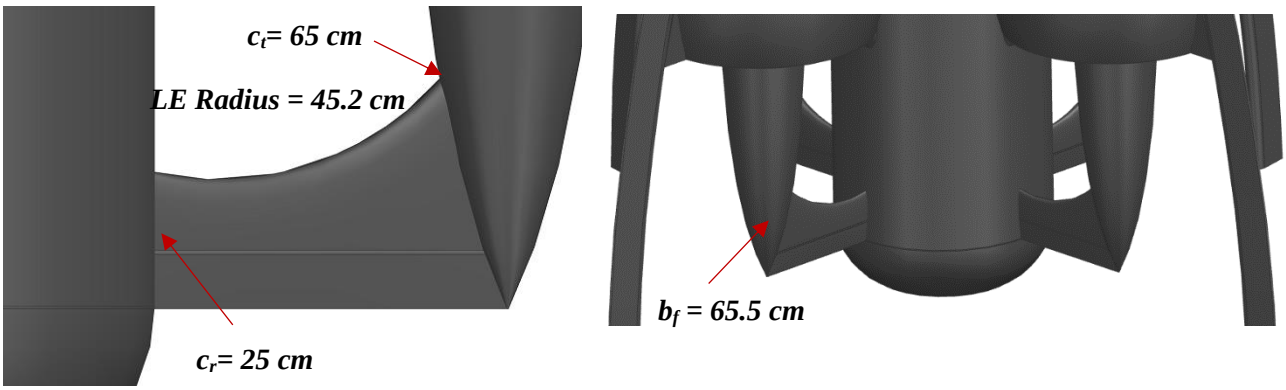

Figure 11.1: Planform and Isometric Views of the Empennage

This reference area was then used to see the affect that the tail has on moving the aerodynamic center location when compared to the aircraft center of gravity. From the analysis in Figure 11.2, the sizing of the tail maintains a desired stable static margin of under 10%.

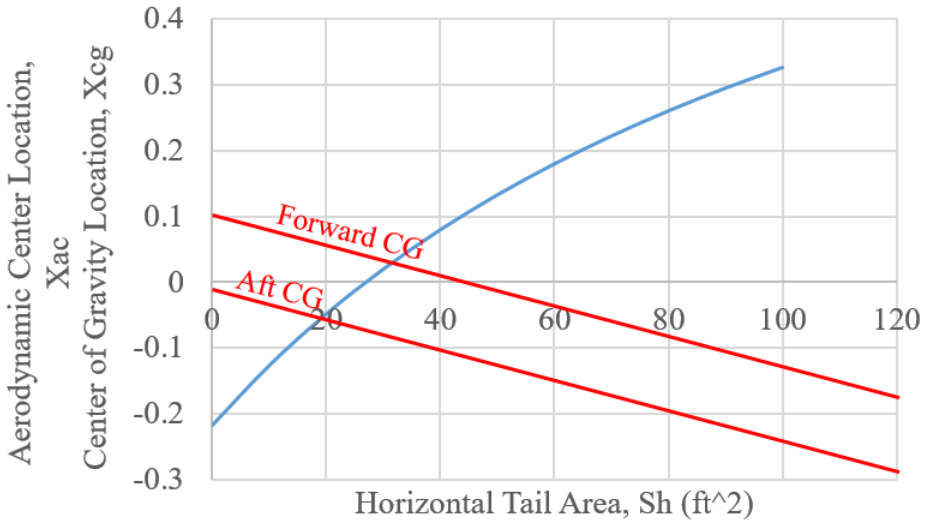

Figure 11.2 Aerodynamic Center Location to Tail Area Relation

12. WEIGHT AND BALANCE ANALYSIS

To allow for good stability and control of the aircraft in flight, the center of gravity must be positioned correctly during all flight stages. To achieve this the payload will be able to be moved independently within the fuselage to match the payload CG to that of the aircraft. To do this, first the CG of the empty aircraft must be found. The first step is to construct estimates of the weight fractions of each individual component of the aircraft. While previous estimates have

given weights for fuel, and engines, and the mission specification details a payload weight, all other components had to be estimated. Thus, the similar in concept coleopter XQ-138 weight fractions have been used as a baseline estimate as it is like a single power pod equivalent in this design. A list of the weight fractions is shown alongside the resulting component weights. With component weights estimated, now attention can be given to CG positions. Because the aircraft is axially symmetric, there are no CG's positioned off the Z axis. Because of the movable payload, the overall CG can be adjusted to always be located at 10% behind the leading edge of the rotor guard lip. From the CAD model the following was found:

Table 12.1: Estimated Weights for Design Components

	Weight Fractions (%)	Weight (kg)	Weight (lb)
Structure & Fixed Equipment	**24.7**	**56.02**	**123.5**
Fuselage & Rotor Guards	18.5	41.96	92.5
Muffler Hard Points	2	4.54	10
Elevons	0.8	1.81	4
Pitch & Yaw Servos	0.3	0.68	1.5
Roll Servos	0.4	0.91	2
Throttle Servo	0.1	0.23	0.5
Undercarriage	1.4	3.18	7
Fasteners & Frames	0.9	2.04	4.5
Servo X-Frame	0.2	0.45	1
Electrical Connections	0.1	0.23	0.5
Propulsion	**48.1**	**109.09**	**240.5**
Moller Engines	24	54.43	120
Starter	1	2.27	5
Throttle Linkage	0.1	0.23	0.5
Fuel	15	34.02	75
Trapped Fuel and Oil	0.2	0.45	1
Fuel tank & Lines	1.2	2.72	6
Muffler	4.6	10.43	23
Rotors	2	4.54	10
SAS/Coms/Power Package	**3.2**	**7.26**	**16.0**
Gyros	0.4	0.91	2
Autopilot	1.2	2.72	6
Receiver	0.4	0.91	2

Power Switch	0.1	0.23	0.5
Substrate & Connectors	0.1	0.23	0.5
Power Conditioning	1.0	2.27	5
Payload	**24**	**54.43**	**120.0**
Primary Payload	22	49.90	110
CG Positioning System	2	4.54	10
MGWTO	100	226.80	500
Woe	62.8	142.4	314

Table 12.2: Component Positions and Weights

	Weight (kg)	FS (cm)	X_cg (cm)	W*X (kg*cm)	Z_cg (cm)	W*Z (kg*cm)
Fuselage & Rotor Guards (4)	30	320	220	6600	0	0
Muffler Hard Points	6	340	240	1400	0	0
Turning Flaps (4)	4	550	450	1800	0	0
Turning Flap Servos (12)	4.4	545	445	2000	0	0
Undercarriage	12	520	420	5000	0	0
Fasteners and Frames	2	360	260	520	0	0
Servo X-Frames	3.1	400	300	930	0	0
Elec. and Mech. Connections	1.1	320	220	240	0	0
RotaPower Engines (4)	56.7	340	240	14000	0	0
Starter	1.2	345	245	290	0	0
Fuel	27.2	345	245	6700	0	0
Trapped Fuel and Oil	0.5	340	240	120	0	0
Fuel Tanks and Lines	4	345	245	980	0	0
Muffler	7.5	340	240	1800	0	0
Rotors (4)	3.6	335	235	850	0	0
IMU/Magnetometer (3)	0.5	160	60	30	0	0
Autopilot	0.3	180	80	20	0	0
Autopilot mount	0.2	185	85	20	0	0
Receivers (3)	0.8	260	160	130	0	0
Navigation Lights	0.2	280	180	40	0	0
ADS-Transponder (3)	0.2	190	90	20	0	0
FCS Battery	2.5	210	110	280	0	0
Sensor Battery	1.5	210	110	170	0	0
Navigation Cameras	0.6	200	100	60	0	0
Primary Payload	50	340	240	12000	0	0
CG Positioning System	6.7	330	230	1500	0	0

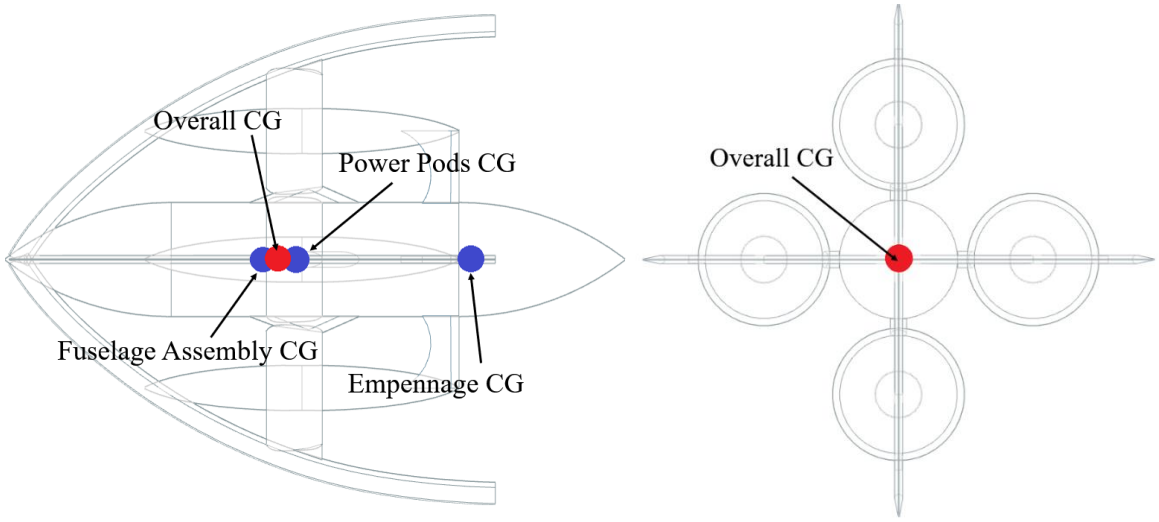

Figure 12.1: View of CG locations on Aircraft

With the weights of the components and the CG locations known, a Weight-CG excursion diagram can be made. Again because of the movable payload and fuel stored near the center of gravity, the position of the overall CG does not greatly change. This is reflected in Figure 12.2.

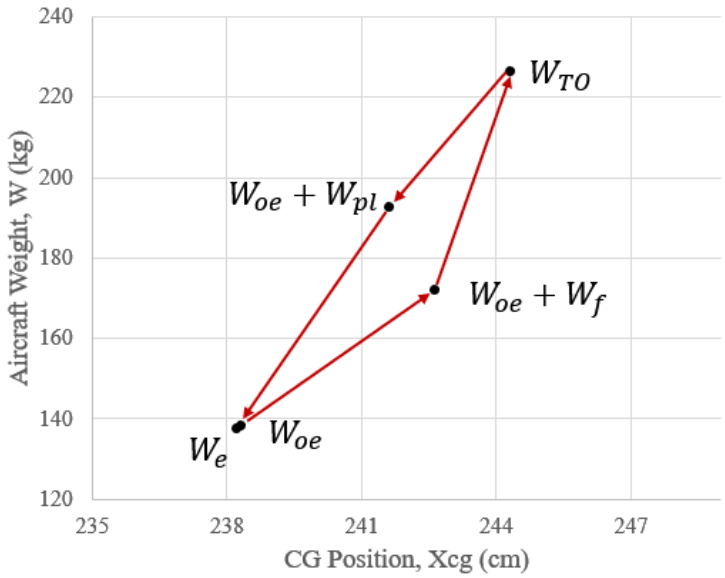

Figure 12.2: Weight-CG Excursion Diagram

13. LANDING GEAR DESIGN

Landing gear is the final component needed for this preliminary design. While classic aircraft designs heavily feature wheels, they always add either complexity in retracting systems or unwanted drag if left out. To circumvent this issue, and to fix a problem left by the fuselage design, an inflatable ballute has been chosen as a replacement for traditional landing gear. While typically used as an airbrake, like in Figure 13.1, this ballute will instead act as flow separation deterrent, similar to the shape attached to the Space Shuttle for transport in Figure 13.2. Affixed to the back end of the fuselage, the ballute consists of a Kevlar bag which is inflated and deflated by the same exhaust line valve system that powers the payload positioning system. Once the aircraft has taken off, the ballute will inflate to full length, completing the fuselage shape into another tangent ogive, drastically reducing flow separation during cruise. When landing, the ballute becomes the first point of contact for the aircraft and acts as a cushion which takes the landing loads, instead of the side arches. In this way heavy loads are avoided on the arches and their structural connections, and they are only needed to stabilize the aircraft once fully landed. This also improves landing ability at unprepared terrain emergency sites.

Figure 13.1: Example of a MK82 Bomb with a Ballute

Figure 13.2 Space Shuttle with Added Tail Piece

As the first point of contact for the aircraft during landing will be the inflatable ballute tail, it will provide a cushioning effect that will lessen the loads the outer arches must take upon landing. To calculate how pressurized the ballute must be to withstand the landing while acting as an air cushion the following calculations shown in Equations 13.1 to 13.4 were run.

$$E_t = \frac{1}{2} W_L \frac{{W_t}^2}{g} \qquad \text{(Eq. 13.1)}$$

$$P_m = \frac{E_t}{n_s N_g (\eta_t s_t + \eta_s s_s)} \qquad \text{(Eq. 13.2)}$$

$$A_b = \pi \frac{{D_f}^2}{4} \qquad \text{(Eq. 13.3)}$$

$$P_{ballute} = \frac{P_m}{A_b} \qquad \text{(Eq. 13.4)}$$

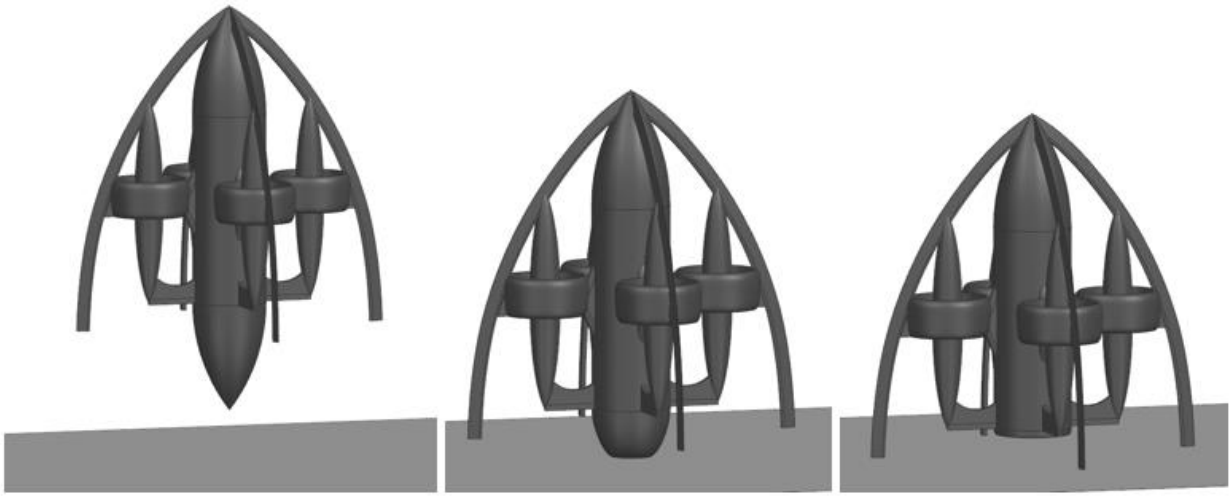

Figure 13.3: Landing Process on Deflating Ballute

By assuming that the stoke of the ballute is half of its total length, and accounting for a maximum possible landing load force of 8 g's, the calculated interior pressure the ballute requires is:

- $P_{ballute}$ = 2900 pa or 0.43 psi.

This pressure is easily reached by simply supplying a small volume of exhaust air from an engine.

14. AIRCRAFT THREE-VIEW

The aircraft outer mold line now complete, a three-view of the design is provided below.

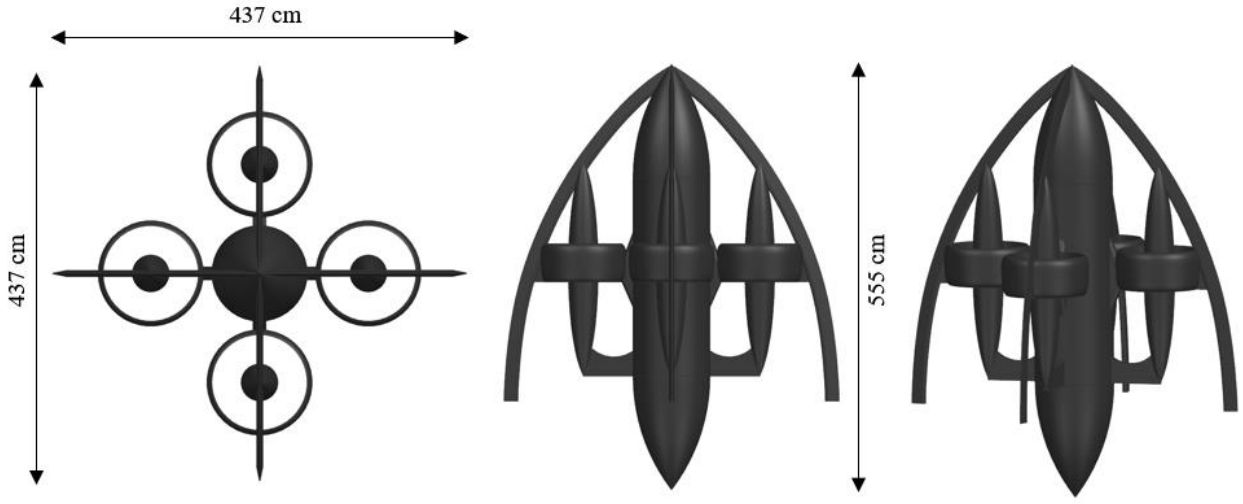

Figure 14.1: Aircraft Three-View

15. V-N AND PAYLOAD RANGE DIAGRAMS

With the preliminary design complete, next the range of its abilities needs to be tested. The aircraft structure must withstand a variety of loads over its service life. These includes loads experienced in flight, shown in the V-n diagram below, but also handling and shipping forces. Rail shipping can cause extremely high loading conditions due to bumping stock. These loads can reach up to 30 g's (ref), far exceeding any other force the structure must endure during flight, which reaches a maximum of only 6 g's during gust loading. Because of this the structure will be overly robust, which also will help increase survivabliilty in case of a wall or cable strike.

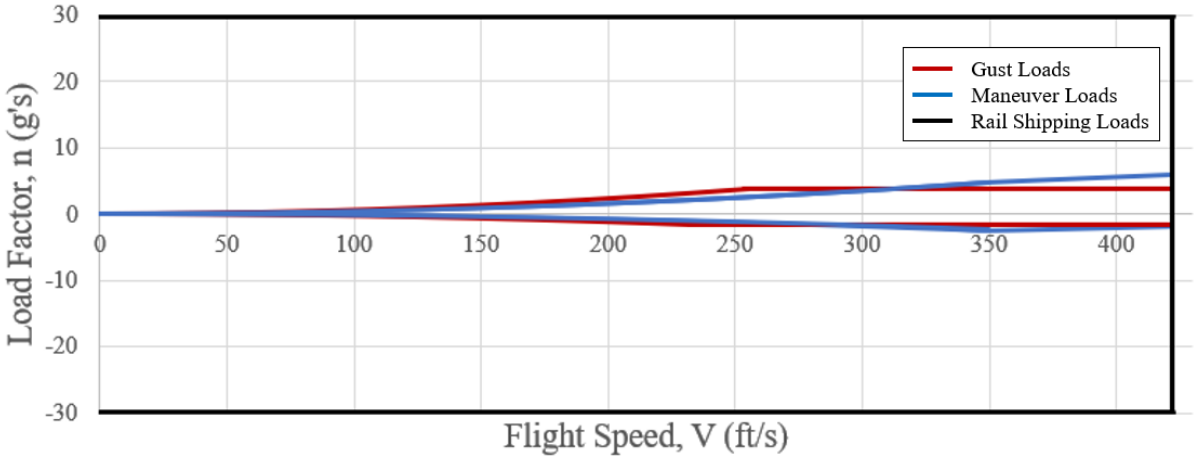

Figure 15.1: V-n Diagram with Rail Shipping Loads Shown

Payload-Range diagrams are an important tool to understand the complete mission capabilities on an aircraft. While the UAV is designed to carry a 50 kg payload for 200km, by replacing part or all of the payload with extra fuel tanks an additional 600 nmi can be added to the range, useful for transporting the aircraft to a launch site nearer a disaster relief effort.

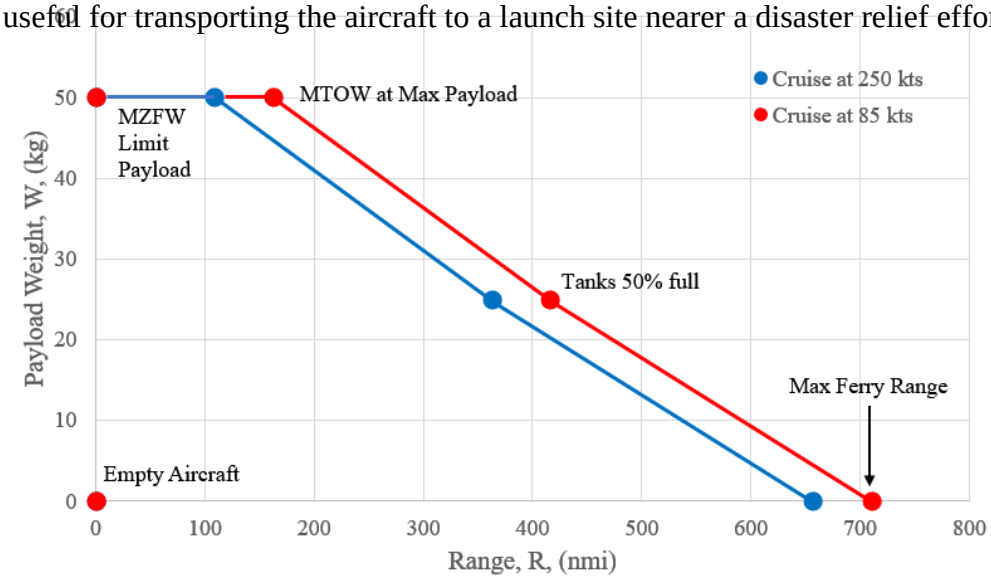

Figure 15.2: Payload-Range Diagram

16. STABILITY AND CONTROL ANALYSIS IN AAA

As the emphasis of this design is maximum safety, the stability and control analysis aims to satisfy Level 1 handing qualities as a Class IV aircraft, during Category A flight. This is the most restrictive stability requirements and meeting them demonstrates a high level of safety inherent in the design. To calculate the flying qualities for the various flight modes the program AAA is used. Within AAA the geometric characteristics of the aircraft were input and analyzed.

Using the output values and the equations Eq.16.1- 16.10, flying qualities can be checked for Phugoid, Short Period, Spiral, Dutch-Roll, Roll, and general handling qualities. To satisfy safe flight, the following ranges were met;

- Phugoid: $\xi_p > 0.04$
- Short Period: $0.35 < \xi_{sp} < 1.30$
- Spiral: $N_\beta L_r - L_r N_r > 0, \quad T_{2S} \sim \infty$
- Dutch-Roll: $\xi_D < 0.05$
- Roll: $\left(\frac{M_q N_r}{M_\alpha} + \frac{I_{yy}-I_{xx}}{I_{zz}} + \frac{N_\beta (I_{xx}-I_{zz})}{M_\alpha I_{yy}}\right)^2 - 4\left(\frac{I_{yy}-I_{xx}}{I_{zz}}\right)\left(\frac{N_\beta (I_{xx}-I_{zz})}{M_\alpha I_{yy}}\right) < 0.$

$$\xi_p = \frac{C_{D_u} + 2C_{D_1} - C_{T_{x_u}} - 2C_{T_{x_1}}}{2.828 C_{L_1}} \quad \text{Eq. 16.1}$$

$$\omega_{n_p} = 1.414\left(\frac{g}{U_1}\right) \quad \text{Eq. 16.2}$$

$$C_T = \frac{T}{\bar{q}S} \quad \text{Eq. 16.3}$$

$$\omega_{n_{sp}} = \sqrt{\frac{Z_\alpha M_\alpha}{U_1} - M_\alpha} \quad \text{Eq. 16.4}$$

$$\xi_{sp} = -\frac{M_q + \frac{Z_\alpha}{U_1} + M_{\dot{\alpha}}}{2\sqrt{\frac{Z_\alpha M_\alpha}{U_1} - M_\alpha}} \quad \text{Eq. 16.5}$$

$$N_\alpha = \frac{\bar{q}SC_{L_\alpha}}{W} \quad \text{Eq. 16.6}$$

$$T_{2S} = \frac{L_\beta ln2}{N_\beta L_r - L_r N_r} \quad \text{Eq. 16.7}$$

$$\omega_{n_D} = \sqrt{\frac{Y_\beta N_r + N_\beta (U_1 - Y_r)}{U_1}} \quad \text{Eq. 16.8}$$

$$\xi_D = \frac{-N_r + \frac{Y_\beta}{U_1}}{2\omega_{n_D}} \quad \text{Eq. 16.9}$$

$$P_{max} = \left|\frac{L_{\delta a}\delta_a}{L_p}\right| \quad \text{Eq. 16.10}$$

17. SENSORS, S&C, & COMS SYSTEM

Figure 9.1 shows a color-coded electrical set-up of onboard electronics and propulsion. A list of onboard electronics and their market names is shown in Table 17.1. In Table 17.1, each item has been hyperlinked with its specifications.

Table 17.1: Electrical Components

Electrical Load Item	Market Name
Receiver (3)	FrSky X8R
Autopilot (1)	MP21283X Triple Redundant
Flight Control Servos (12)	Hitec RCD® HRC32805S
Navigational Lights	elechawk LED Light Strip
ADS-B Transponder	PING-200SR
IMU (3)	MOTUS
nav. Cameras (day and night)	MS5000S
Engine Starter	1.4 kw high torque starter motors for early models

Table 17.2 shows the electrical load summary times and energy required for the logistics mission. This table will be used to size the FCS and Sensor battery. Note, in Table 17.2, the power columns represent the power consumption of one single market item whilst the energy columns represent the total energy required to run every onboard electrical load item during each flight stage. Additionally, the starter generator power consumption in Table

17.2 is an estimate that assumes a 100A at 12V pulse that lasts for 10 seconds during start-up. In addition, the power for the lights was calculated assuming a 4W consumption per foot.

Table 17.2: Electrical Load Summary Times for Logistics Mission

Electrical Load Item	30 Sec Preflight/Start-up		30 sec T/O & Climb		26 min Cruise		2 min Landing	
	Power (W)	Energy (J)	Power (W)	Energy (J)	Power (W)	Energy (J)	Power (W)	Energy (J)
Receiver (3)	0.5	45	0.5	45	0.5	2300	0.5	180
IMU (3)	1.4	126	1.4	130	1.4	6500	1.4	500
Autopilot (1)	9	270	9	270	9	140000	9	1080
Flight Control Servos (12)	0.05	18	3	13000	3	660000	35	50400
Navigational Lights (6 – 1.8 ft strips)	7.2	1300	7.2	1300	7.2	67000	7.2	5184
ADS-B Transponder (3)	1	90	2	180	2	9400	2	720
Cameras (night/day) (14)	1.2	504	1.2	504	1.2	26200	1.2	2020
Engine Starter	1400	14000	0	0	0	0	0	0

Table 17.3: Electrical Load Summary Times for Logistics Mission

Battery Type	**Market Name**
Flight Control System (FCS) Battery	TATTU 7000mAh 4s 25c Lipo Battery
Sensor Battery	Lumenier 205mAh

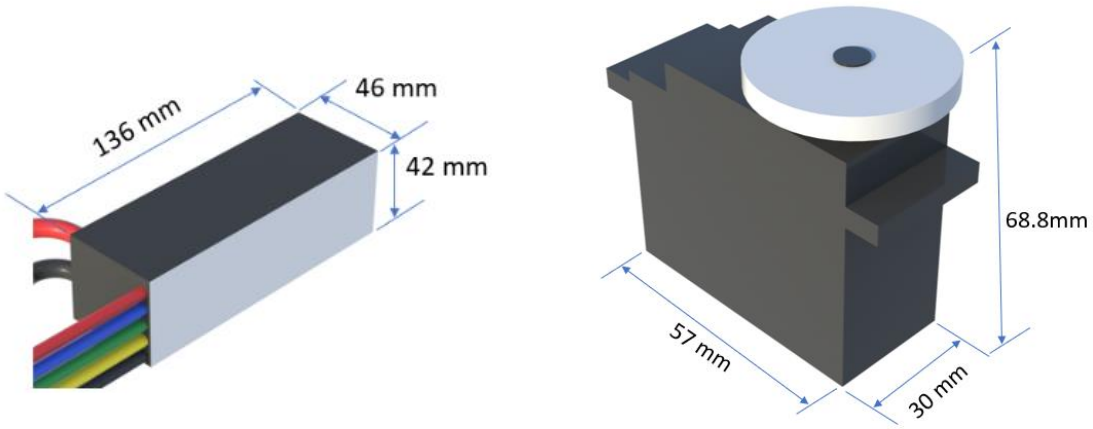

Figure 17.1: Dimensioned Electrical Components

A proposed wiring diagram of all the connections and systems necessary to operate the aircraft autonomously is shown in the following figure.

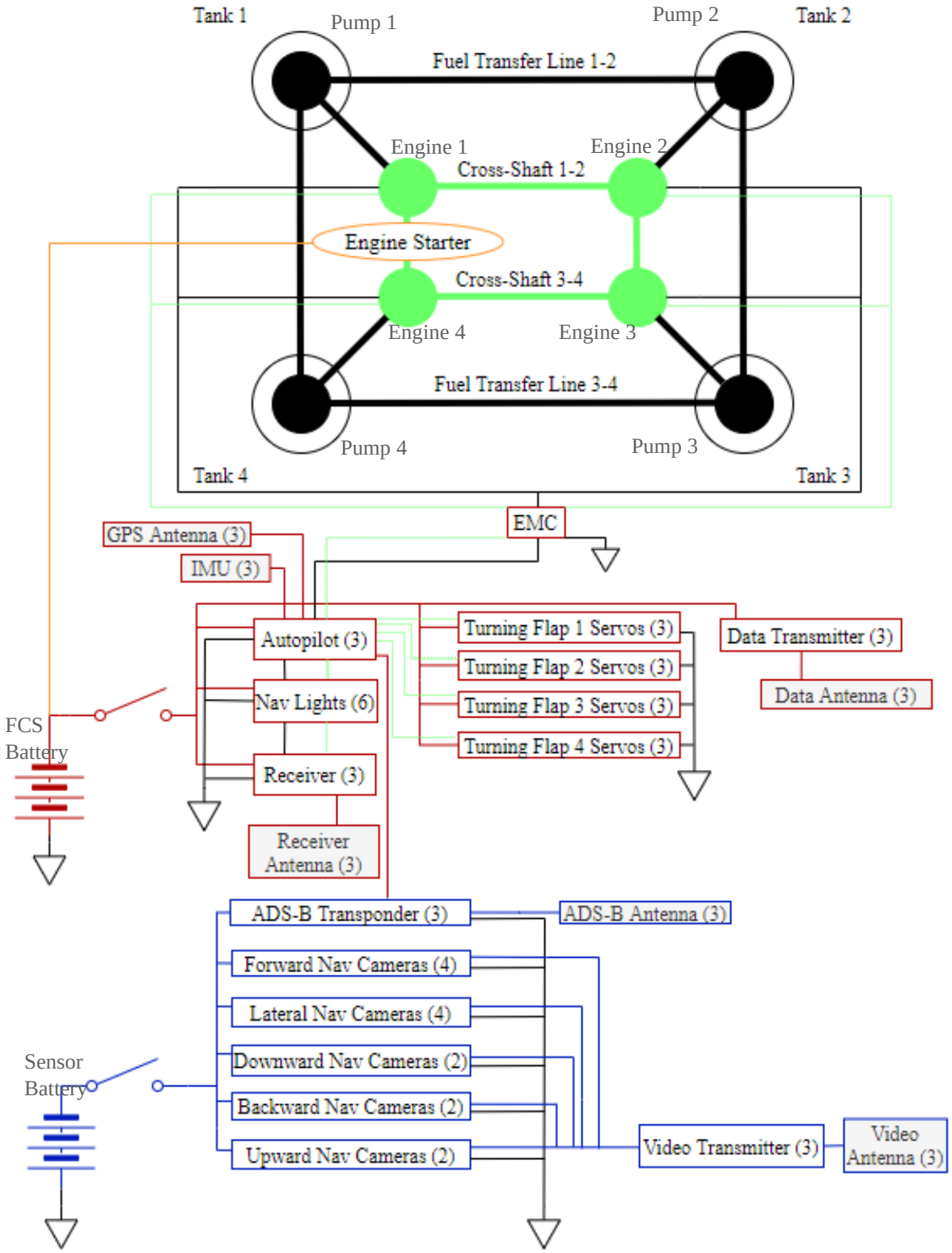

Figure 17.2: GNC Block Diagram

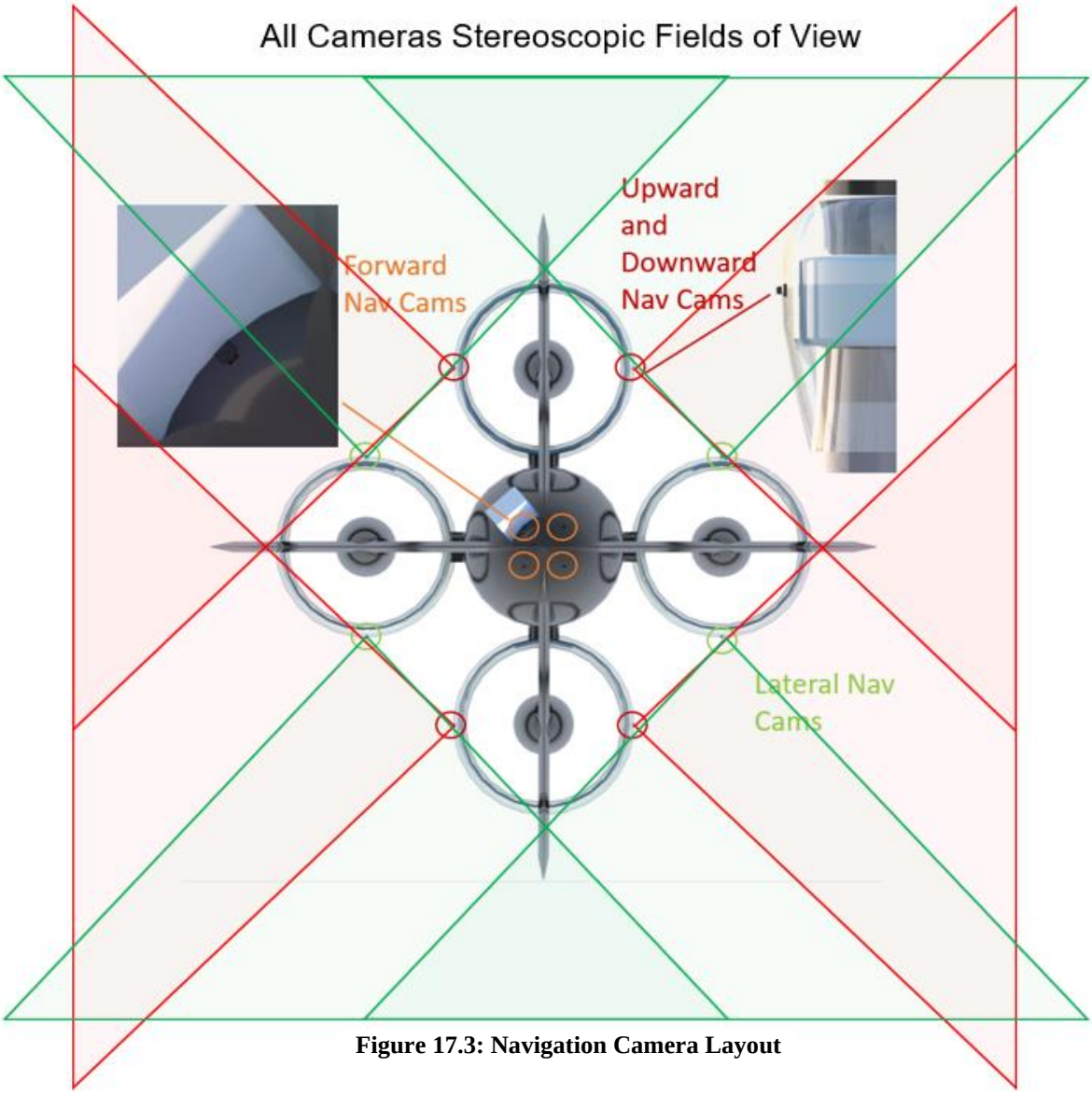

Figure 17.3: Navigation Camera Layout

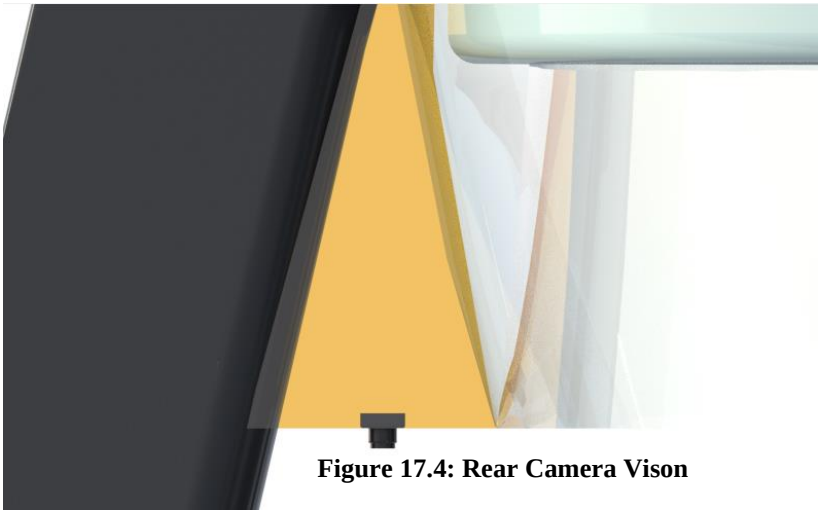

Figure 17.4: Rear Camera Vison

18. LAYOUT OF MAJOR SYSTEMS

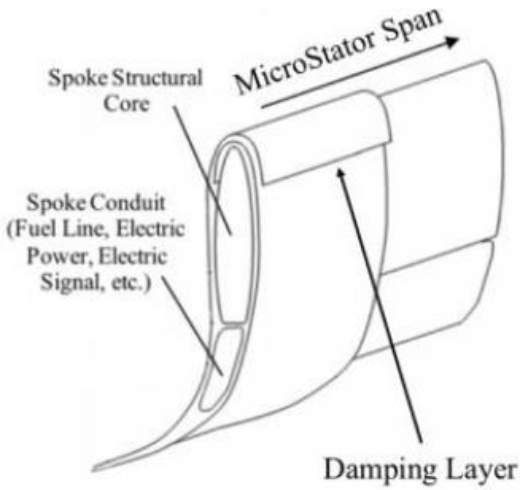

Figure 18.1: MicroStator Inner View (Ref. #)

The engines will take aviation gasoline, 100LL. This fuel has a density of 6.8 lbs per gallon. From the weight sizing code, the aircraft needs 70.6 lbs of fuel or 10.4 gallons of aviation gasoline to complete the logistics mission. The fuel tanks have been designed to carry 5.2 gallons of fuel each combing for a total of 20.8 gallons. This is so the aircraft can trade off cargo weight for more fuel weight and higher ranges if ever needed. It is also important to note that these are bladder fuel tanks. Bladder fuel tanks are necessary to prevent foamed fuel which would be a problem for a convertible body-tilt aircraft due to fuel sloshing in a regular fuel tank. The fuel tanks have been strategically placed in the rotor guards to minimize aircraft CG excursion

The CG positioning system consists of airbags at the top and bottom of the aircraft. These airbags draw exhaust air to inflate and deflate position the payload so that the aircraft CG excursion is minimal.

The GPS antennae have been placed strategically so that at least one GPS antenna points towards the sky at all times. The receiver antenna has been placed so that a person in the loop will be able to take control of the aircraft in case of a catastrophic failure at any time.

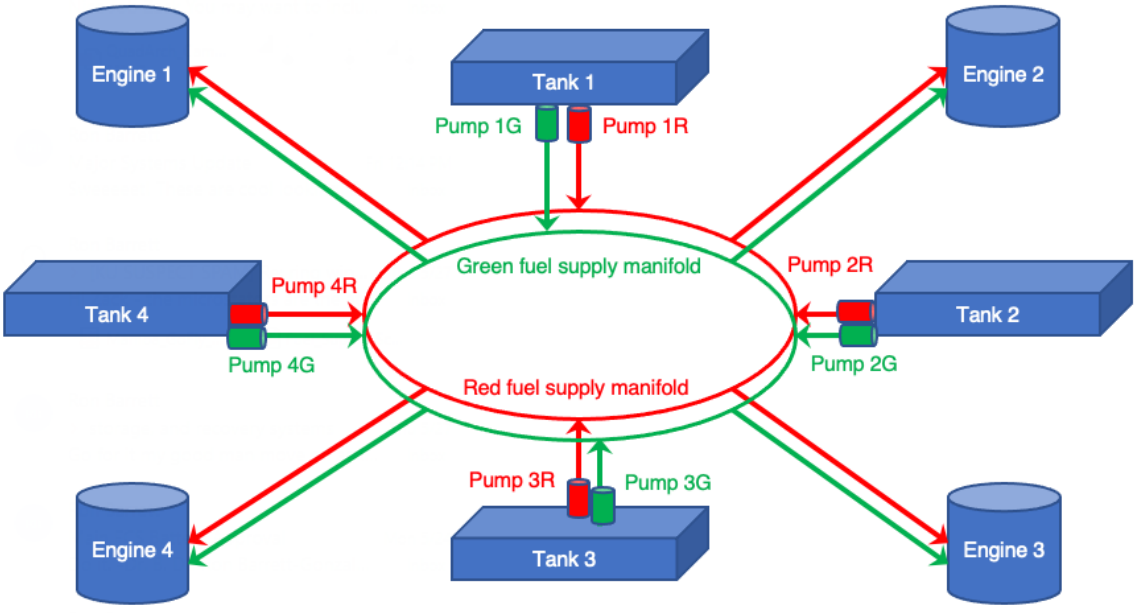

Figure 18.2: Fuel System Schematic

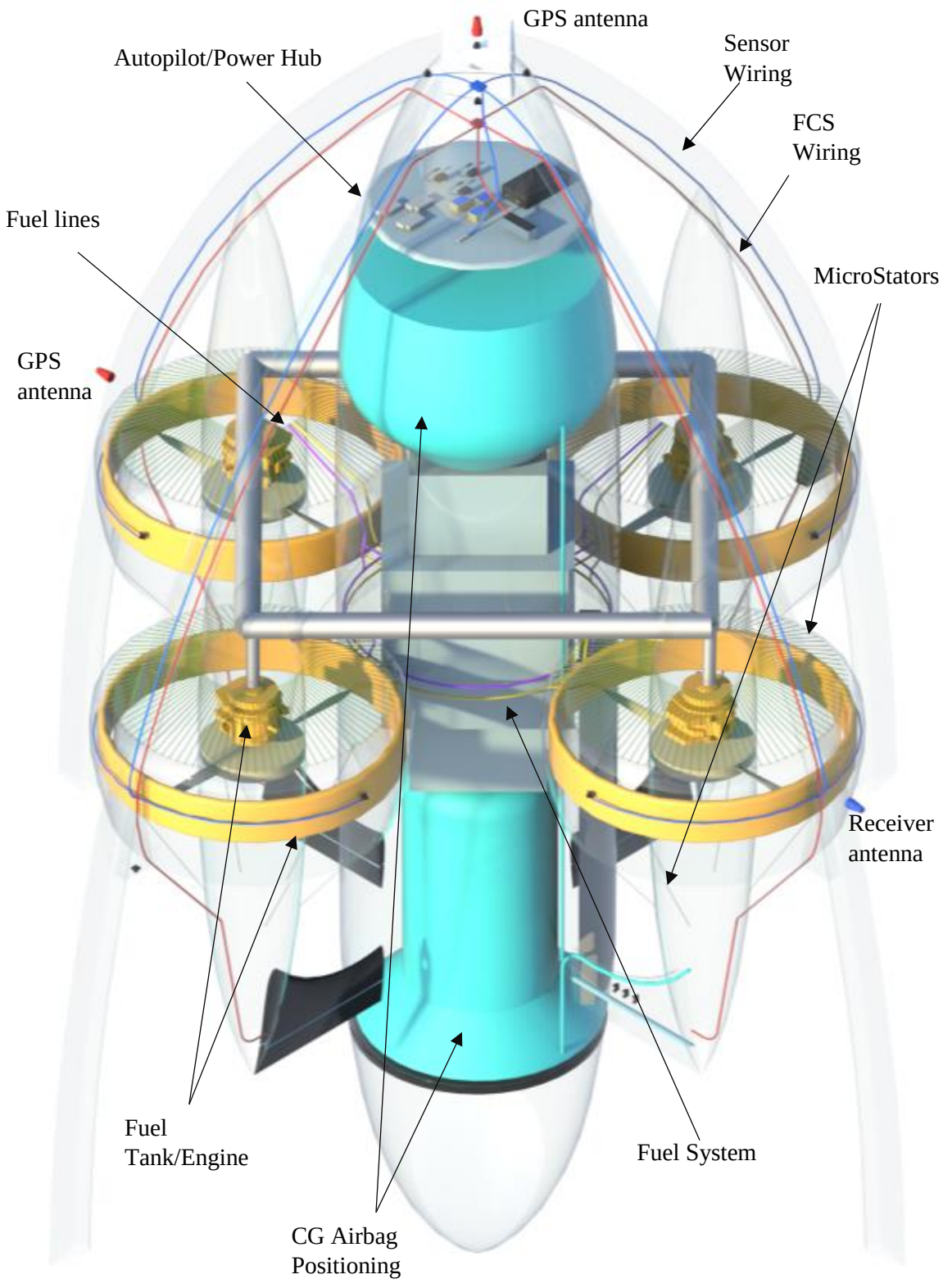

Figure 18.3: Layout of Major Internal Systems

19. STORAGE AND RECOVERY SYSTEMS

The missing third dimension not shown in Figure 19.1 is the duct diameter (3.3 ft). Therefore, the shipping container for shipping component no. 1 will have dimensions of 7.75’ x 15’ x 4.25’. The shipping container for shipping component no. 2 will have dimensions 15’ x 4’ x 4’. The shipping components can be seen in their packages in Figure 19.3 and Figure 19.4. The standard flat-bed is around 8.5 ft wide and 48-53 ft long. The shipping arrangement can be seen in Figure 19.4. It is important to note that a forklift will be necessary to load the crates onto the flat-bed trailer. In addition, if there is an emergency, (two adjacent engines go out) the recovery parachute system can be seen in Figure 19.2. The parachute chosen was sized for light sport aircraft at a maximum takeoff weight of 660 lbs. It weighs 15.0 lbs and has dimensions of 11.0 x 9.8 x 6.7 in.

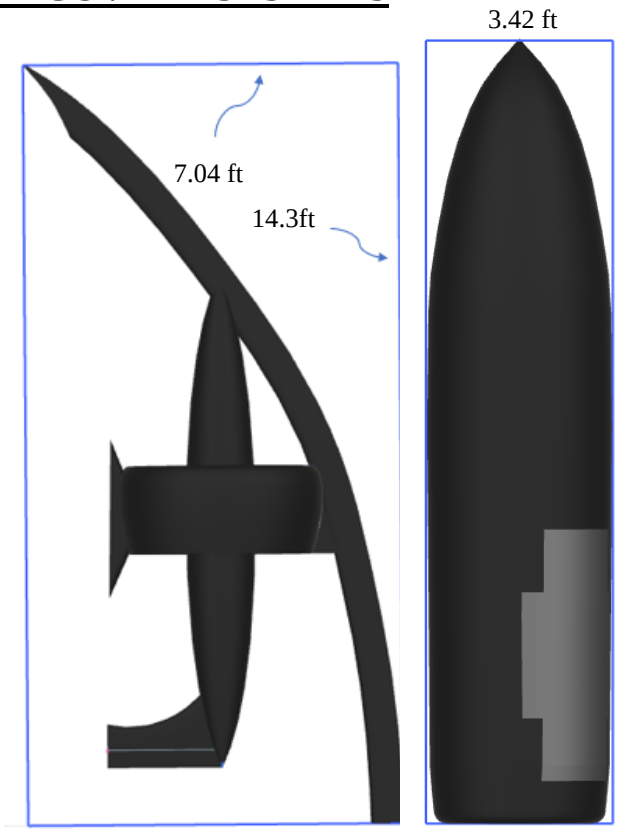

Figure 19.1: Shipping components no. 1 (left) and no. 2 (right)

Figure 19.2: Recovery System

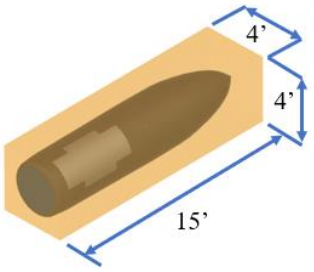

Figure 19.3: Shipping component no. 2 packaged

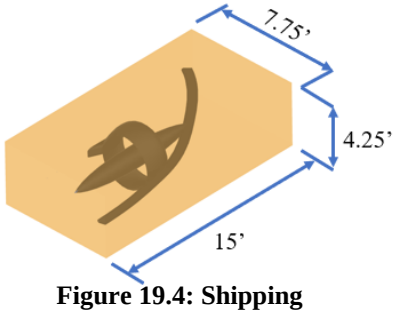

Figure 19.4: Shipping component no. 1 packaged

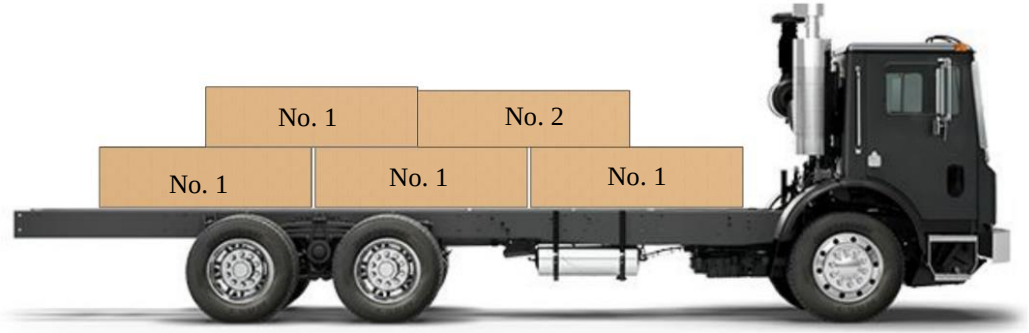

Figure 19.5: Flatbed Shipping Arrangement

20. SITUATIONAL RENDERING

Figure 20.1 shows how the payload will enter and exit the aircraft.

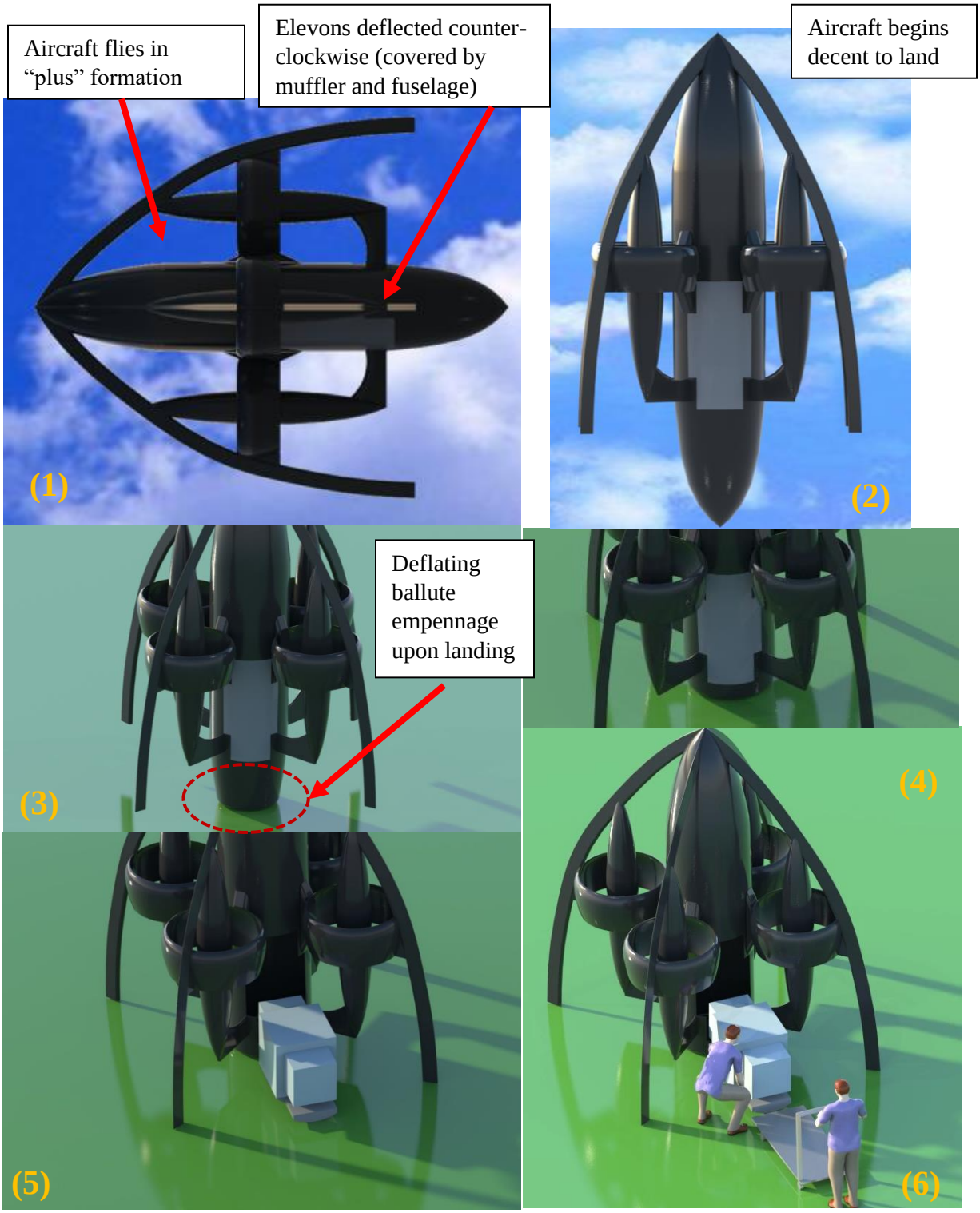

Figure 20.1: Payload Egress/Ingress Mechanism

21. GROUND SAFETY, FLIGHT SAFETY, AND CERTIFICATION

Safety is the highest focus of this design. To ensure that the aircraft is as safe as possible, several different techniques have been implemented to reduce the risk of civilian harm in both ground and flight operations. In ground operations, the main concern is the possibility of a person being injured by contact with the aircraft, specifically with rotating parts. To minimize this, micro stators have been used for each of the four ducted fans. These stators act as a wire guard over the top of the propeller and do not allow any human body part to come in contact with a rotating component. As a bonus, microstators also reduce the noise production of the power pods by transmitting higher frequency noise, outside the human audio spectrum. See Figures 21.1 – 21.3. For microstator stress and CFD analysis, and a real-world noise level test.

For flight safety, the main issue is the chance for cable strike, especially during takeoff and landing procedures. Do alleviate the possibility of gusts blowing the hovering aircraft into nearby cables, the design features a roll cage like structure that protects the engines and fuselage from direct strikes. The roll cage also increases the survivability of the aircraft should it encounter a wall strike. This will be a major factor in achieving a certification base.

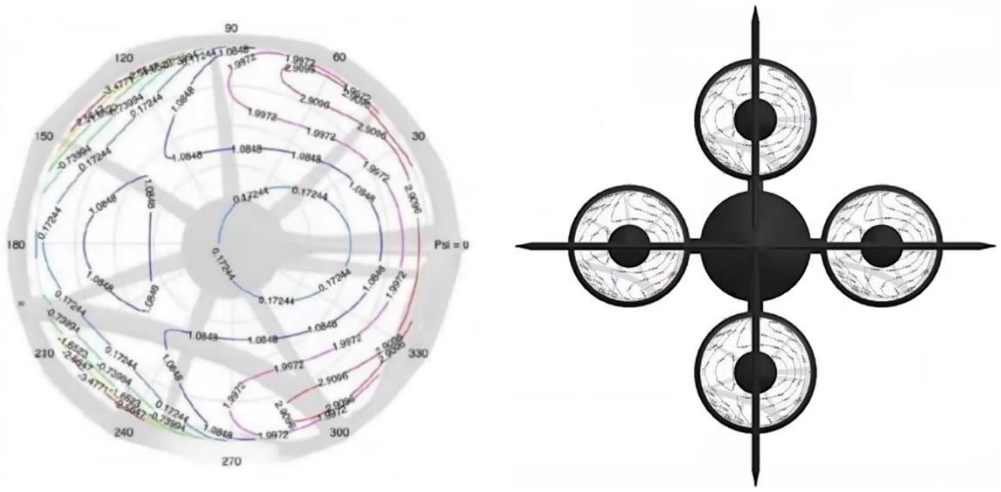

Figure 21.1: CFD Analysis of MicroStators

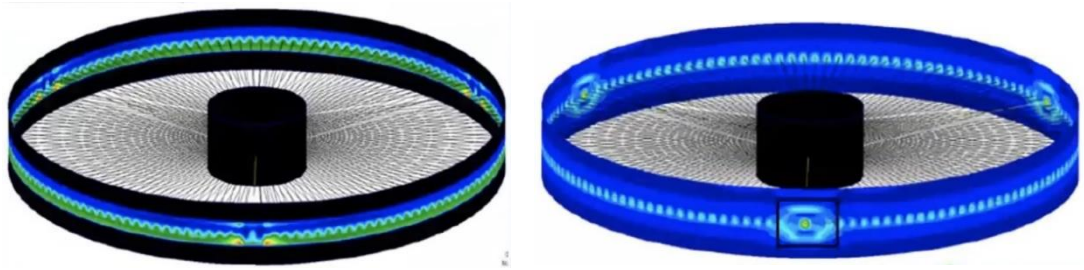

Figure 21.2: PATRAN Analysis of MicroStators

Figure 21.3: Sound Test of Micro Stators

22. COST ANALYSIS

Approximating the cost of the design is an important step to illustrate its viability in the market. To estimate the total life cycle cost and the cost per individual unit, the method detailed by Roskam in Aircraft Design: Part VIII Chapters 3 and 4 will be used (Ref. 20). By simply imputing the ampere weight and the max speed the aircraft will travel at, an estimate for total aircraft costs can be found. Tables of the used assumed values are recreated below:

Table 22.1: Assumed Values for RDTE Cost

Variable	Assumption
Airframe Engineering and Design Cost (pg. 22-28)	
W_{ampr}	121 lbs: 24.7% of the XQ-138 based on weight fractions
V_{max}	250 kts: dash speed from V-n diagrams
N_{rdte}	5 aircraft: 1 structural, 1 ground vibration test, 1 hover test, 2 transition test
F_{diff}	1.5: convertible aircraft of this kind have been made before
F_{cad}	1
R_{er1990}	$62: Roskam pt. VIII Figure 3.3
CEF_{1990}	140: Roskam pt. VIII Fig 2.7
CEF_{2020}	250: Roskam pt. VIII Figure 2.7
Development Support and Testing Cost (pg. 29)	
$CEF=CEF_{2020}$	250
Flight Test Airplanes Cost (pg. 29-33)	
N_e	4: four ducted fan engines
N_{st}	2: one for static and one for crash test
N_p	0
C_{er}	$35,000: The cost of each 40hp engine was $45,000. Scaling based on the hp, the approximate cost per engine will be $35,000
C_{pr}	0
$C_{avionics}$	$350,000: based on reference numbers
$R_{m,r1990}$	$34/hr: Roskam pt. VIII Figure 3.4

F_{mat}	2: using advanced composites
N_{rr}	8: Assuming around 100 aircraft can be produced per year
$R_{t,r1990}$	$44/hr: Roskam pg. VII Figure 3.5
Flight Test Operations Cost (pg. 34)	
F_{obs}	1: No stealth requirements
F_{space}	2: Factor added into account for the increased airspace needed to flight test the aircraft for safety reasons
Test and Simulation Facilities Cost (pg. 35)	
F_{tsf}	0: No extra facilities needed
RDTE Profit (pg. 35)	
$F_{pro,r}$	0: Assuming non-profit for liability reasons
Cost to Finance the RDTE Phases (pg. 36)	
$F_{fin,r}$	0.05: Assuming 5% interest rate

Table 12.2: Calculated Values for RDTE Cost

Variable	Calculated Value	Eqn. #, pg. #
Airframe Engineering and Design Cost (pg. 22-28)		
$MHR_{aed,r}$	16160 hrs	3.2, 24
R_{er}	$111/hr	3.6, 28
$C_{aed,r}$	$178,900	3.3, 24
Development Support and Testing Cost (pg. 29)		
$C_{dst,r}$	$12,210,000	3.7, 29
Flight Test Airplanes Cost (pg. 29-33)		
$C_{(e+a),r}$	$1,470,000	3.9, 30
$MHR_{man,r}$	$70,450	3.11, 31
$R_{m,r}$	$60.70	
$C_{man,r}$	$4,277,000	3.10, 31
$C_{mat,r}$	$57,470,000	3.12, 31
$MHR_{tool,r}$	51350 hrs	3.14, 33
$R_{t,r}$	$78.60	
$C_{tool,r}$	$4,035,000	3.13, 33
$C_{qc,r}$	$556,000	3.15, 33
$C_{fta,r}$	$67,810,000	3.8, 29
Flight Test Operations Cost (pg. 34)		
$C_{fto,r}$	$1,926,000	3.16, 34
Test and Simulation Facilities Cost (pg. 35)		
$C_{tsf,r}$	$0	3.17, 35
RDTE Profit (pg. 35)		
$C_{pro,r}$	$0	3.18, 35
Cost to Finance the RDTE Phases (pg. 36)		
$C_{fin,r}$	$4,187,000	3.19, 36
C_{RDTE}		
C_{RDTE}	$87,920,000	3.1, 21

Assuming a reasonable production run of two hundred aircraft with an industry standard 6% financing cost and 10% profit to break even, the estimated acquisition cost would be $510,000 per aircraft. To operate such an aircraft would require fuel, a ground operator, a ground takeoff station, and general service. Together these can be assumed to cost about $280 per hour of operation. Finally, assuming that each aircraft has a life span of 1,000 flight hours, the life cycle cost would thus be $790,000 for an aircraft. At a lifetime price of under a million dollars, this aircraft could potentially have applications beyond emergency medical supply delivery, and thus could be used in other markets such as a rapid high-end civilian delivery service.

23. SCALE MODEL FABRICATION AND TESTING

23.1 WIND TUNNEL AND FREEFLIGHT TEST AIRCRAFT DESIGN

Given the unusual configuration of the Asklepios aircraft, along with the complications coming from powered lift, separated flow and full aircraft conversion, it was determined that wind tunnel and flight testing could be more easily accomplished with more accurate results than a CFD analysis given the time and budget available. Accordingly, a powered 1/27 scale model was built to verify aerodynamics and aeromechanics associated with the design.

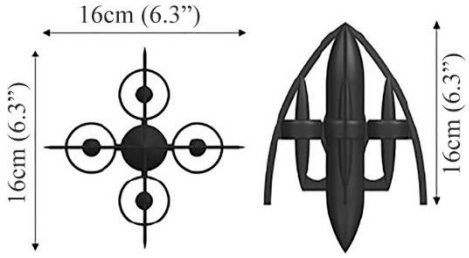

Figure 23.1.1: Wind Tunnel and Freeflight Test Aircraft Dimensions

23.1.1 GENERAL CONFIGURATION AND GEOMETRY

The 1/27 scale Asklepios wind tunnel and freeflight test aircraft was designed and built to the dimensions at right. The aft fuselage ballute was made to be a removable ogive depending on what kind of testing was underway. The 40mm ducts were constructed from 0.5mm thick injection molded rotor guards. The assembly was designed in several major parts. The upper arch and fuselage assembly connects to the mid-section at the rotor guards. The mid-section structurally attaches to the lower fuselage at the powerplants. The removable aft fuselage ogive nests within the lower fuselage tube independently.

23.1.2 STRUCTURAL MATERIALS

The wind tunnel and freeflight model will be made out of flight weight materials so that it may be used for multiple purposes. The arches will be composed of Kevlar-reinforced balsa to lend robustness and crashworthiness to the aircraft. The power pod ogives will be constructed from balsa as will the tail

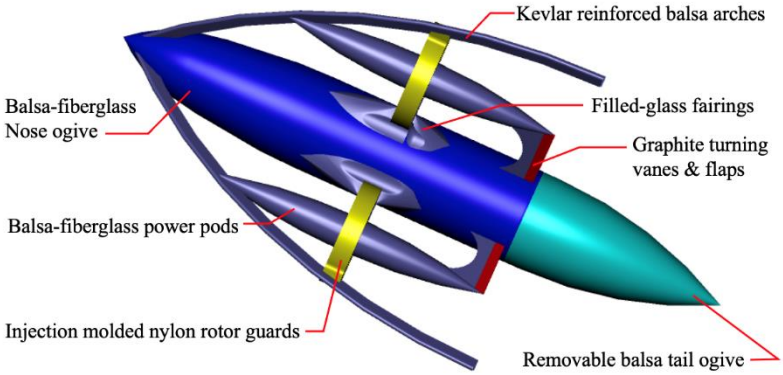

Figure 23.1.2: Wind Tunnel and Freeflight Test Aircraft Materials

ogive. The nose ogive will be made from glass-reinforced balsa. The fairings around the aircraft will be composed of glass-bead filled epoxy. The central body sections will be balsa and flightweight polycarbonate. The rotor guards as well as the rotors will be made from injection molded nylon.

23.1.3 PROPULSION ASSEMBLY

The propulsion assembly consists of four 40mm ducted fans with four-bladed rotors in each one powered by 8.5 mm dia x 20mm long brushed motors @ 15,000 kV. The aircraft is powered by a single 1S 3.7V 500 mAh LiPo battery with up to 25C discharge.

23.1.4 UNDERCARRIAGE AND LANDING ASSEMBLY

The undercarriage assembly is built from a Kevlar-balsa composite, tapered towards the ends of the arches. The arch terminations included a polyurethane dip end so as to cushion landing shocks. The full-scale landing ballute system is also planned, but for a stage of flight testing that will occur after submission of this report given time constraints.

23.1.5 POWER CONDITIONING AND GNC SYSTEM

Power conditioning will be handled via a Blade Inductrix power-GNC board. The aircraft is designed to be flown via 1st and 3rd person flight modes. When flying in the wind tunnel, the camera assembly was removed (as it was unnecessary and reduced the total amount of power available to the powerplants).

23.2 WIND TUNNEL AND FREEFLIGHT TEST AIRCRAFT FABRICATION

The Asklepios was built in several major assemblies and designed to be robust and crashworthy. The major structural components were made from fiber-reinforced balsa. To accommodate impact loads, the arches were reinforced with Kevlar. Glass microspheres were used in conjunction with style 120 fiberglass cloth to aid force transfer to the nose ogive assembly. Figure 23.1.3 shows the test frame.

23.2.1 PROPULSION ASSEMBLIES

Figure 23.2.1: Test Aircraft Propulsion Frame

The propulsion assembly was based on a 40mm dia. frame powered by four 8.5 x 20mm 15kV motors. Figure 23.2.1 shows the frame itself. The aircraft was built around the propulsion frame with the outer arches being structurally attached by shock

Figure 23.2.2: Injection-Molded Nylon 40mm Rotor for Test Aircraft

mounts to the rotor guards. The motors were measured as consuming from 0.3A to 3.8A during peak draw conditions at 3.5 - 3.7V (peak power of 14W).

23.2.2 STRUCTURAL ELEMENTS

Figure 23.2.3: Formation of Balsa-Kevlar Arch Assembly

The balsa arches were fabricated in the same way that planks of wood for shipbuilding are formed: They were soaked for a day in water, then slowly bent via a series of rubber bands around a properly shaped aluminum mandrel. Drying occurred at an elevated temperature till the balsa took the prescribed shape. The pieces were stripped to 2mm widths and finished to an airfoil profile after curing. The right side of Figure 23.2.3 shows the arches being co-cured with Kevlar lines on the extremities in a flashing tape jigging process. The fuselage assembly was designed to be removable and replaceable so as to facilitate wind tunnel mounting and removal as well as conversion to flightworthy aircraft following wind tunnel testing.

Figure 23.2.4: Balsa Ogive- Fuselage Assembly

23.2.3 GNC ELECTRONICS, TRANSMITTER, RECEIVER & FINISHED AIRCRAFT

The Blade Inductrix board used was just one of several that were planned for the model. In the end the Inductrix board was the preferred board because of its low weight and tight form factor as well as versatility. Testing indicated a quiescent current draw of only 200 - 220 mA which was more than acceptable for the prescribed power budget. The entire finished aircraft (minus the various balsa tail cones) can be seen in Figure 23.2.6. The aircraft empty weight includes all components except the battery and tail cone. The aircraft top-level aircraft weights are as follows:

Table 23.2.1: Major Aircraft Weights

Empty	**52.0g**	**1.83oz**
Tail Cone	5.0g	0.18oz
Battery:	12.7g	0.45oz
MGWTO:	69.7g	2.46oz

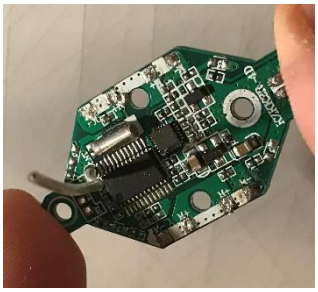

Figure 23.2.5: GNC, Receiver & Transmitter Board

Figure 23.2.6: 1/27th Scale Asklepios Wind Tunnel and Flight Test Aircraft

23.3 WIND TUNNEL TEST AIRCRAFT SETUP

23.3.1 STING BALANCE & QUADRANT

Figure 23.3.1: Test Aircraft Mounted in the University of Kansas 3 x 4' Subsonic Tunnel

The model was tested with a precision 3 component balance rated to 10 lbf in force, 3 ft-lbf in torques with 0.1% precision. Temperature compensation was automatically adjusted at an update rate of 1 Hz. The sting dynamics were accounted for with a low-pass filter of 0.2 hz cutoff as testing was conducted in a quasi-static mode. A full-span quadrant was used to sweep angle of attack from 0 to 90° of body pitch attitudes in 10 deg. increments. The Sting balance and quadrant assembly was rated ultimately to 100lbf of load in any direction (well below the forces experienced). All flight testing was conducted in the "+" position (rather than the "X" position) so as to decouple controls and allow for span maximization. For testing beyond 90° angle of attack (simulating descending/tail slide conditions), the model was mounted backwards on the same sting such that the tail was facing upstream.

23.3.2 CONTROL COMMANDS

Three major test commands were used. The first was the quadrant control which incremented the aircraft pitch attitude in 10 deg. increments +- 0.1 deg. The second was wind tunnel speed which varied from 0 ft/s through 50 kts. Given that the model was a Froude-scaled model, the 250kt top-end speed at 1/27 scale was translated to a tunnel speed of 48kts. Motor RPM and power was controlled remotely by the transmitter which was assessed by integrally mounted tachometers mounted to two of the rotors. For the purposes of these tests, the turning vane flaps were kept in the neutral position given limited tunnel test time.

23.3.3 DATA ACQUISITION, TEST MATRIX AND TUNNEL TEST TIME

Wind tunnel force and moment data were acquired at 100 Hz by a National Instruments digital data acquisition system. Force and moment data were filtered using a 1 Hz low pass filter (time averaging), but with statistical deviations in data being recorded. Lift, drag, and pitching moments were measured using the force balance described in Section 23.3.1. 18 hours of wind tunnel test time were recorded gathering data at the 570 data points listed below before time constraints cut testing short. The following test conditions were performed.

Table 23.3.1: Wind Tunnel Test Matrix

	Minimum	Maximum	Increment
Angle of Attack	0°	180°	10°
Tunnel Speed	0kts	50kts	10kts
Power Setting	0% Pmax	100% Pmax	25% Pmax

23.3.4 TUNNEL AND MODEL SAFETY

The principal concern of nearly all wind tunnel testing is the safety of the personnel involved, then the tunnel, then the object to be tested. A tunnel safety review was conducted by the Test Safety Review Committee prior to testing. Loads at 2x those which were predicted to be experienced were applied to the model prior to testing while on the sting to ensure structural integrity.

23.4 WIND TUNNEL TEST RESULTS

23.4.1 TUNNEL CORRECTION FACTORS

The model was kept more than 10 rotor diameters and 3 spans away from walls during testing at all times. Wind tunnel test data was corrected for wall effects using the techniques of Ref. 23. Figure 23.3.2 shows the wind tunnel test conventions.

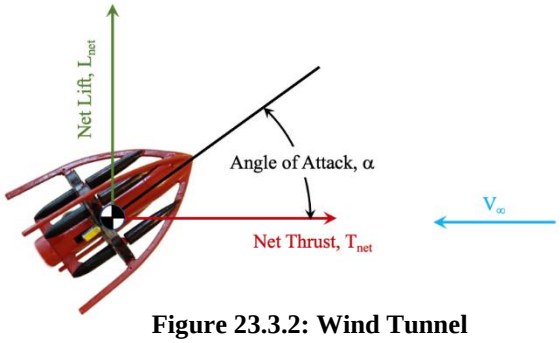

Figure 23.3.2: Wind Tunnel Test Conventions

23.4.2 STATIC ANGLE OF ATTACK, SPEED AND POWER SWEEPS

570 points of data were collected over two weeks of testing at the University of Kansas 3 x 4' low speed wind tunnel. The data was corrected for wall effects. Rather than nondimensionalize the data, the data was left in dimensional form as the definitions of normalization areas can vary widely depending on what community is being addressed. Should the reader wish to normalize the data, the rotors used were 40mm (1.57") in diameter, within 45mm (1.77mm) diameter ducts. The span-to-span rotor guard projected area measured 12cm x 1cm (4.72" x 0.39"). The total lateral projected area in the "+" flight condition was 147cm2 (22.8

sq.in) with a tip-to-tip arch span of 16.0cm (6.3"). The maximum power consumption recorded was 14 W/motor, a total of 56W. Power flows corresponding to 1 through 100% were measured as a fraction of the 56W of electrical power consumed per motor. Wind tunnel testing shows full transition capability being maintained through 50kts under 1g flight (which equates to a Froude-scaled speed of 260kts) under full power at just over 10 deg. angle of attack.

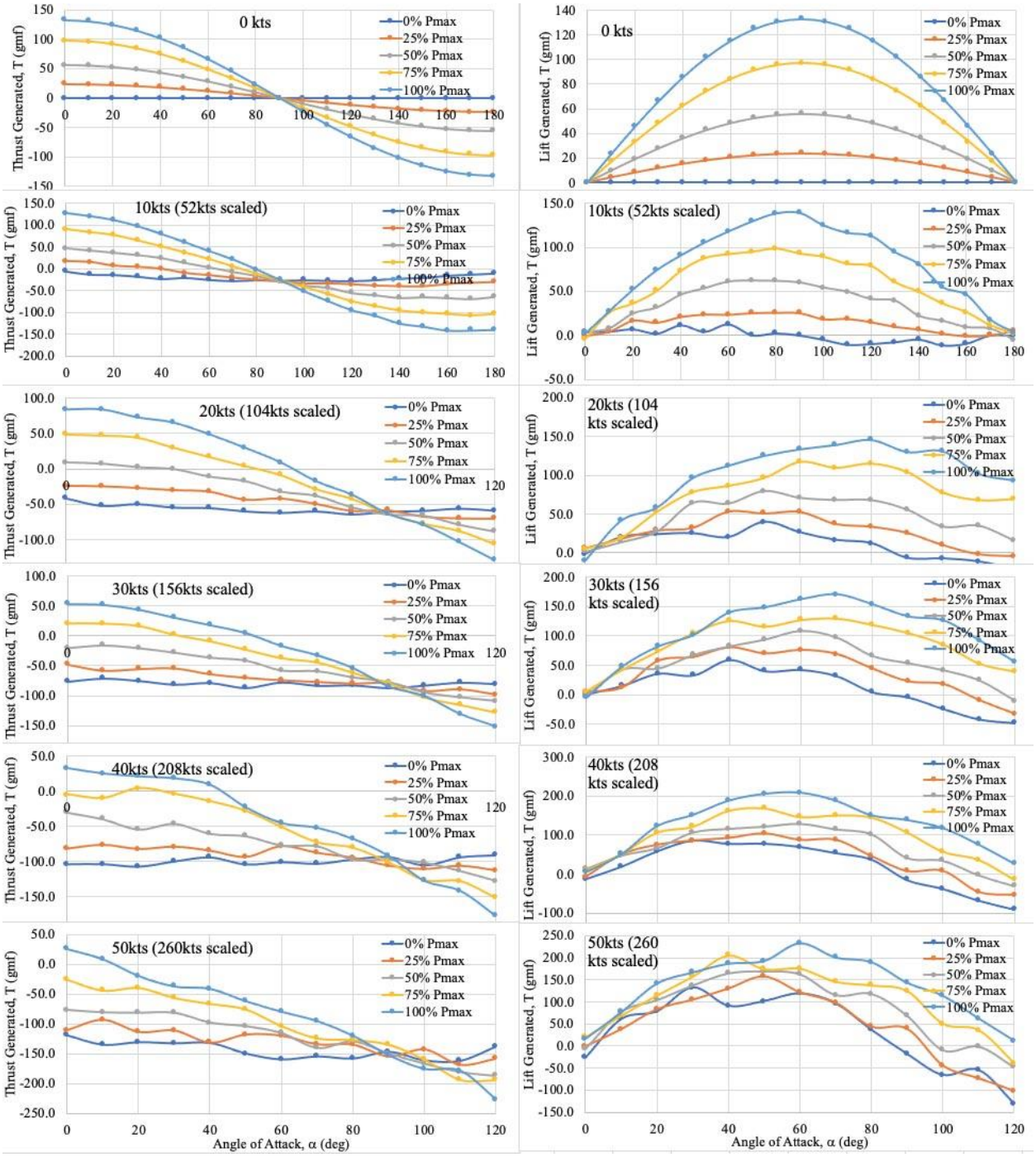

Figure 23.4.1: Wind Tunnel Test Data Through 50kts (260kts Froude Scaled)

The aerodynamic center location was challenging to get under some circumstances as the noise in the data was considerable, especially at high angles of attack. Of course, at 0 deg. angle of attack, it is similarly erratic. Figure 23.4.2 shows the position of the A.C. as a function of angle of attack with its considerable error bars showing the total range of the data. It is suspected that large shed vortices off the fuselage is contributing to the extremely large scatter at high angles of attack. These shed structures are then ingested into the downwind duct which then in turn influences the total pitching moment. Nonetheless, the data shows that the aerodynamic center is within 25% of a rotor diameter of the rotor guard lips. In all circumstances, the aircraft had more than enough control power to execute pitch control through 20 kts and 30 deg. angle of attack. Beyond 20 kts, 30 deg. α, control power limits were seen at high angles of attack. Testing the control power envelope will have to be deferred to full transition corridor establishment which is beyond the scope of this document given time and wind tunnel test budget constraints.

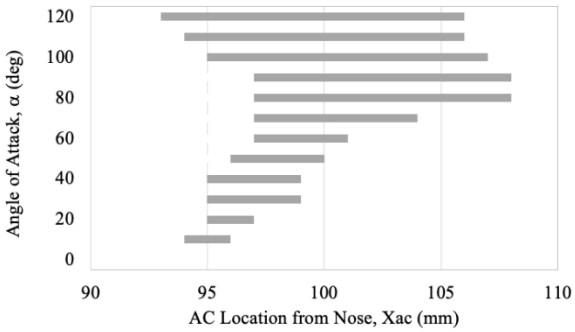

Figure 23.4.2: AC Location with Angle of Attack

23.5 FREEFLIGHT TEST SETUP

The 1/27th scale Asklepios model was built to fly with a maximum thrust-to-weight ratio in excess of 2:1. Indoor flight testing was limited as the threats of wall-suction and hard-impact crashes were ever-present. Outdoor testing was conducted at the University of Kansas West Campus and sandlot volleyball Athletics facilities. Both tall grass on West Campus and sandlots cushioned the hard landings that the aircraft endured during transition testing.

23.6 FREEFLIGHT TESTING

23.6.1 HOVER TESTING

Figure 23.6.1: Flight Path Departure at 150kts, 5.9g Pullup

Hover testing was conducted both in and out of ground effect. Hover in ground effect (HIGE) was achieved at 18% full throttle, or a power setting of 10W of power consumption by the motors. Hover out of ground effect (HOGE) consumed 22 - 24% full throttle or 12.3 - 13.4W. Wall suction effects were noted as being profound. The reader is referred to the flight video (https://vimeo.com/557298319) to see the aircraft performance in hover out of ground effect.

23.6.2 TRANSITION TESTING

The Asklepios flight test aircraft achieved full transition four times during flight test prior to the submission of this report. The flight profiles flown were akin to those established in Ref. 24. Two forms of transition entry were tried, both worked. From Ref. 24, a method to establish a solid transition corridor had been established years ago in the XQ-138 program. Figure 23.6.2 shows what happens when a transition is attempted too quickly -- the convertible aircraft pitches up uncontrollably and tumbles as separated flow off the fuselage interacts with both flight controls and propulsor(s). Once time allows, the map of the full Asklepios transition corridor boundary as shown in Figure 23.6.3 will be established. In the meantime, two different entry techniques were employed during flight testing: i.) Hover-climb, then dive to entry, ii.) Hover-climb direct entry. One technique was used for transition back from high speed flight to hover-mode flight: Zoom climb to burn off airspeed, then back down slowly. This was the only method that has been shown to safely work for fully convertible aircraft like the Asklepios as shown in Figure 23.6.4.

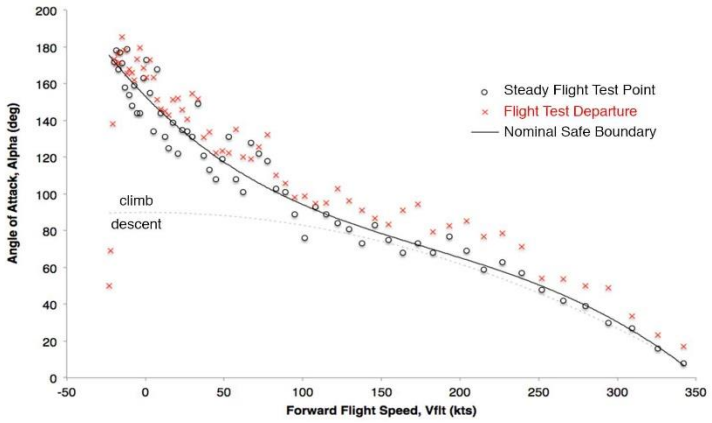

Figure 23.6.2: V-α Departure Boundary for Transition Corridor Establishment

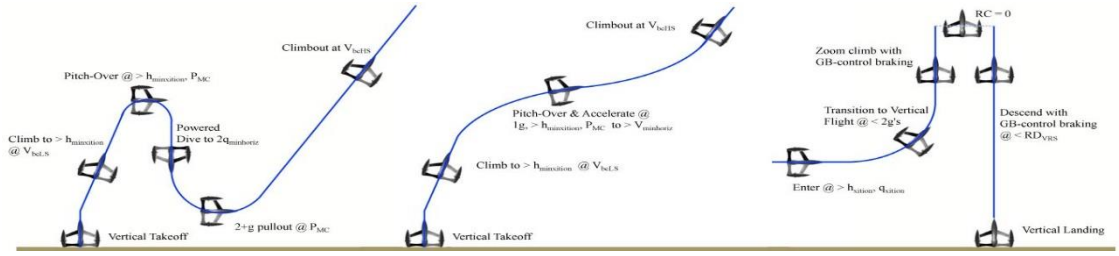

Figure 23.6.3: Two High Speed Conversion Entry Transitions Used, One Exit Transition

23.6.3 HIGH SPEED TESTING

High speed flight testing was conducted at the Jayhawk Model Masters Field in Douglas County. Speeds were measured by passing measured time-gate poles. Top transitioned flight speeds were 46, 48 and 52 kts.

23.6.4 RAIN TESTING

To meet the submission deadline, flight testing was forced to take place in inclement weather. The aircraft was water hardened and the powerplants did not lapse with changes in humidity (unlike internal combustion powerplants). It was noted that during rainfalls in excess of 1cm/hr (0.4"/hr) that the power required to hover both in and out of ground effect was reduced by approximately 10% each time. It is thought that the increase in mass flow rate through the rotors increased their lifting capacity.

23.6.5 WIRE-STRIKE TESTING

Because the UAV will, necessarily, operate at low altitudes in close proximity to many different kinds of electrical wires, wire strike qualification is a must for this kind of aircraft. The Chief of the Small Aircraft Directorate of the FAA put it well:

Drones Operating below 500 ft must be qualified for wire strike.

They have and will continue to strike wires at an alarming rate no matter how good their wire detection or avoidance systems are. What is more is that they must do so safely with neither wire break nor crash.

-Wes Ryan, Chief, FAA Small Aircraft Directorate 2018

Wire strike testing was conducted with three different configurations of drone: i.) Open Rotor, ii.) Closed Rotor, iii.) Asklepios. The purpose of the test was to show that the Asklepios can survive direct wire strikes at high speeds while the other configurations are upset to the point that they crash. By using Froude-scaling principles, five 3mm diameter rubber lines simulated the stiffness of transmission lines at a 1/27th scale. The five lines were placed between two posts at 20 ft (540ft scaled distance). The three aircraft were flown at the lines between 10 and 30 kts (52kts and 156kts scaled speed). The Asklepios struck the lines at the full 156kt scaled speed with only an 18 deg. flight path angle deviation induced and no flight departure. The reader is encouraged to see just how catastrophically the other configurations are affected by wire strike and how well the Asklepios survives wire strike (https://vimeo.com/557352330).

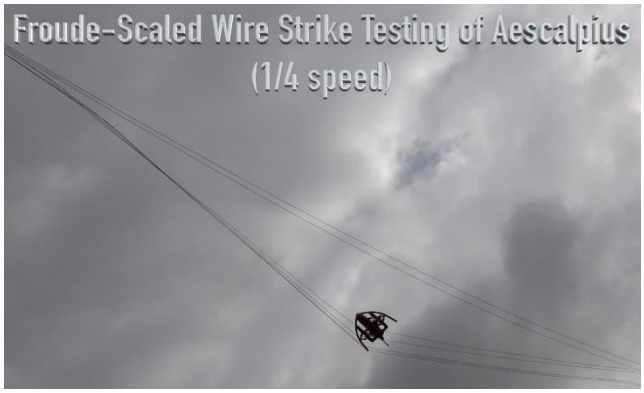

Figure 23.6.4 Froude-Scaled Wire Strike Flight Testing of Open-Rotor, Closed-Rotor and Asklepios Drones

23. CONCLUSION

The RFP called for a design that could safely and efficiently carry a 50kg load to emergency sites up to 200km away quickly and autonomously. As of 2021, there is currently no extant aircraft that could fulfill this purpose well, as the market for UAVs is split between extremely light weight package delivery concepts and large urban air taxis. Because of this, a new aircraft was designed from the ground up for this report using and building off concepts of previous successful aircraft. The converged solution was a Patent-Pending convertible body-tilt aircraft with four engines, a self-positioning payload system, and a wire strike guard/roll cage with a landing gear ballute. It can reach the maximum FAA allowable travel speed of 250 kts for the specified altitude, can travel over 700 nmi in ferry flights, and has numerous safety measures that limit any kind of danger of the public being exposed to the aircraft. Additionally, the design was built as a $1/27^{th}$ scale model and shown to perform up to standards in wind tunnel and freeflight tests.

24. REFERENCES

1. “2025 Unmanned Vertical Lift for Medical Equipment Distribution (38th Annual Student Design Competition 2020-2021 Request for Proposal (RFP)),” *Vertical Flight Society.*
2. "Hewitt-Sperry Automatic Airplane." Wikipedia, The Free Encyclopedia. *Wikipedia, The Free Encyclopedia,* 2 Jan. 2021. Web. 9 Feb. 2021.
3. "Microdrones md4-3000." GPS World, *website,* [gpsworld.com]. 5 May. 2020. Web. 9 Feb. 2021.
4. "Volocopter 2X." Wikipedia, The Free Encyclopedia. *Wikipedia, The Free Encyclopedia,* 5 May. 2020. Web. 9 Feb. 2021.
5. "Yamaha R-MAX." Wikipedia, The Free Encyclopedia. Wikipedia, The Free Encyclopedia, 23 Jan. 2021. Web. 16 Feb. 2021
6. “PHANTOM 4 RTK Specs,” *DJI*, Web. 15 Feb. 2021.
7. Monti, Chris, “Phantom 4 RTK changes everything! The 5 reasons why,” *Drone DJ*, 3 Dec. 2018. Web. 15 Feb. 2021.
8. Dukowitz, Zacc, “Yuneec Rolls Out RTK Satellite Navigation for Their H520,” *UAV Coach*. 7 2018. Web. 15 Feb. 2021.
9. “YUNEEC H520 SPECIFICATIONS,” *The Drone Pro Shop, 21 Jan. 2018.* Web. 15 Feb. 2021.
10. Dinh, Van, “How much does the DJI Matrice 200 V2 series drone cost?” *Can Drone* 14 Oct. 2020. Web. 15 Feb. 2021.
11. “MATRICE 200 SERIES Specs, *DJI*, Web. 15 Feb. 2021.
12. “Matrice 600 Pro [Price]” *DJI*, Web. 15 Feb. 2021.
13. “MATRICE 200 SERIES Specs, DJI, Web. 15 Feb. 2021.
14. “Top agriculture spraying drones: DJI Agras MG-1 vs Yamaha RMAX” *Drones On Video.* Web. 15 Feb. 2021.
15. “Yamaha's RMAX - the worlds most advanced non-military UAV,” *New Atlas* Web. 15 Feb. 2021.
16. “FAZER and FAZER R [Specifications],” *Yamaha*. Web. 15 Feb. 2021.
17. “Drone Delivery.” *Fehr and Peers*. Web. 15 Feb. 2021.
18. “The Use of Small Unmanned Aircraft by the Washington State Department of Transportation”
19. Roskam, Jan, Airplane Design: Part I: Preliminary Sizing of Airplanes, DAR Corporation, Lawrence, KS, 1997.
20. Roskam, J., “Aircraft Design: Part 1: Preliminary Sizing of Airplanes”, Digital ed., DAR Corporation, Lawrence, KS, 2003, pp. 6 – 23.
21. “Rotapower Specifications” Freedom-Motors, Website *https://freedom-motors.com/freedom_rotapower.html*, 28 Feb. 2021.
22. J. Barlow, W. Rae and A. Pope, Low-Speed Wind Tunnel Testing (3rd Edition), New York, NY: John Wiley and Sons, 1999.
23. R. M. Barrett, " Hybrid Aircraft Aerodynamics and Aerodynamic Design Considerations of Hover to Dash Convertible UAVs," in Advanced UAV Aerodynamics, Flight Stability and

Control: Novel Concepts, Theory and Applications, New York, NY, Wiley, 2017, pp. 423-446.